

# Decoding quasars: gravitationally redshifted spectral lines!

Nimisha G. Kantharia  
National Centre for Radio Astrophysics,  
Tata Institute of Fundamental Research,  
Post Bag 3, Ganeshkhind, Pune-411007  
nkprasadnetra@gmail.com

September 2016

**This version includes errata and comments in the 9 pages appended to the original paper.**

## Abstract

Further investigation of data on quasars, especially in the ultraviolet band, yields an amazingly coherent narrative which we present in this paper. Quasars are characterised by strong continuum emission and redshifted emission and absorption lines which includes the famous Lyman  $\alpha$  forest. We present irrefutable evidence in support of (1) the entire line spectrum arising in matter located inside the quasar system, (2) the range of redshifts shown by the lines being due to the variable contribution of the gravitational redshift in the observed line velocity, (3) existence of rotating black holes and of matter inside its ergosphere, (4) quasars located within cosmological redshifts  $\sim 3$ , (5)  $\gamma$  ray bursts being explosive events in a quasar. These results are significant and a game-changer when we realise that the absorbing gas has been postulated to exist along the line-of-sight to the quasar and observations have accordingly been interpreted.

In light of these definitive results which uniquely constrain the quasar structure, we need to drastically revise our understanding of the universe built on the faulty assumptions of observed redshifts of quasars having an entirely cosmological origin and the absorption lines arising in the intervening medium.

## Keywords

quasars: general, absorption lines, emission lines, supermassive black holes; gamma ray burst: general; galaxies: high redshift

## 1 Introduction

Quasars are a well-observed and well-studied subgroup of objects generally known as active nuclei - we refer to quasi-stellar objects as quasars in this paper. However, they famously remain one of the least understood objects. The study which identified quasars (Schmidt, 1963) reported wide emission lines ( $\sim 50\text{\AA}$ ) on a strong blue continuum in 3C 273. The lines could only be identified if a redshifted velocity component was included although the object had

a star-like appearance. Quasars have spurned extensive research but continue to intrigue even after 50+ years of discovery. Quasars show rich observational signatures which includes strong thermal emission in the ultraviolet (and optical) and a power law continuum emission which dominates the optical to infrared bands and continuing in the radio when detected. Their line spectra show the presence of wide emission lines and numerous absorption features spanning a range of velocities and widths. Some of the observed properties of active nuclei, in particular quasars, can be summarised to be:

- Flat or power law continuum emission from radio to ultraviolet wavelengths. Enhanced ultraviolet emission referred to as the 'blue bump' or 'uv upturn'. Many active nuclei also detected in X-rays.
- Quasar spectra are characterised by broad emission lines and narrow/broad absorption lines. BL Lac objects show a featureless continuum with only a few showing spectral lines. Seyfert 1 galaxies show broad emission lines while Seyfert 2 galaxies show narrow emission lines.
- High ionization lines such as doublets of C IV (1548.188\AA, 1550.762\AA), S IV (1393.755\AA, 1402.770\AA), N V (1238.808\AA, 1242.796\AA), O VI (1031.928\AA, 1037.619\AA) are detected from many active nuclei especially quasars. Low ionization lines such as C II (1335\AA), Fe II (2383\AA, 2586\AA), Si II (1260\AA), Mg II (2795.528\AA, 2802.704\AA) are also detected in the spectra of many active nuclei. These lines are detected either in emission and/or absorption in the quasar spectrum.
- Quasar spectra show a host of redshifts with the emission line redshifts being the largest. Absorption lines span a range of redshifts.
- Many active nuclei show variability especially quasars, blazars and Seyfert 1 galaxies.

While there is general agreement that a supermassive black hole is the central object in all active nuclei, rest of the details remain perplexing at best. It is instructive to glimpse the exciting research that quasars sparked

due to their exotic nature as captured by their observations. Soon after quasars were identified (Schmidt, 1963), the debate on whether these objects were extragalactic and very distant or whether these were Galactic or in the neighbourhood has been going on. Schmidt (1963) and Greenstein & Schmidt (1964) concluded that quasars were distant extragalactic objects. The controversy arose since the large observed redshifted velocities of the spectral lines, if interpreted to indicate Hubble expansion, would make quasars very distant objects. This, then, led to the observed magnitudes translating to very high luminosities for the quasars which had, hitherto, not been observed in any extragalactic object. However, there was a group of astrophysicists who were convinced observations indicated that quasars were local and the redshifts were intrinsic. Arp (1967) suggested that radio sources were associated with nearby peculiar galaxies (Arp, 1966) or bright galaxies (e.g. Arp, 1974). In fact a few such pairs were also found to be physically connected by a bridge (e.g. NGC 4319 and Mrk 205; Arp, 1971). However the local origin did not find favour with most astronomers. One major problem with the local origin and association of quasars with nearby galaxies were the distinct redshifts noted for the quasar (high) and the nearby galaxy (low). Since one of the explanations was that quasars are ejected from nuclei of galaxies (e.g. Arp, 1967), the quasars can show large redshifts. However in this scenario, the quasars would show both redshifted and blueshifted velocities wrt to the nearby galaxy whereas the quasars always showed a redshift wrt to the nearby galaxy. This essentially ruled out the ejection origin for the redshift and an hitherto unknown non-velocity intrinsic origin for the redshifts of quasars was postulated. Arp (1974), Burbidge (2007a) and others continued to advocate the scenario of quasars being local objects and the observed redshifts having an intrinsic origin. In this paper, we revisit the quasar redshifts and present evidence for a sizeable intrinsic redshift component in quasar spectra.

Another perplexing observational result noted around the same time was the arrangement of galaxies in the Coma cluster along bands in the redshift-magnitude diagram which was especially significant when the nuclear redshifts and magnitudes were plotted (Tift, 1972, 1973). This result, in addition to a periodicity observed in the velocity differences in pairs of galaxies (Tift, 1980) suggested that the velocities were quantised in factors or multiples of  $\sim 72 \text{ kms}^{-1}$  (e.g. Tift, 1980). Although these results are not yet understood, its interesting that this value is close to the currently accepted value of the Hubble constant. Since the Hubble constant gives the velocity difference between two galaxies separated by 1 Mpc, the Hubble law can be understood as quantifying the radial velocity distribution of galaxies in space or in other words ‘redshift quantisation’. In fact, it is interesting that Tift had estimated a value for the Hubble constant without realising it. Obviously, observational astronomy was throwing up several puzzling results which were difficult to understand. We present a possible explanation for the redshift-magnitude bands in the paper.

Most of the astronomical community has currently accepted the cosmological origin of redshifts of quasars and observations have been examined with this implicit assumption. Observations which could not be explained like Tift’s bands and Arp’s quasar/galaxy associations were considered to be faulty or spurious which is alarming since even if one did not agree with their interpretation, these were observational results by solid astronomers and needed to be scientifically investigated. A careful study clearly brings out the fantastic nature of quasars and one senses that the unique properties of quasars are likely extreme signatures of an active nucleus. In this paper, we present our study which provides strong evidence to a sizeable internal contribution to the observed redshifts of quasars. We show that one of the physical processes considered for the origin of the observed high redshifts by Schmidt (1963); Greenstein & Schmidt (1964) is indeed the most plausible explanation.

We start with a study of the origin of the large observed velocity shifts of the lines in a quasar spectrum followed by the ultraviolet continuum emission. Then we suggest a structure for the quasar which can explain most ultraviolet observations within the framework of known physics, discuss other active nuclei and variability and end with some concluding remarks.

## 2 Quasars

Quasars have been observed at redshifts ranging from  $\sim 0.1$  to  $\sim 7$ . Since the identification of quasars from emission lines detected at high redshifts, with the first being 3C 273 (Schmidt, 1963), their study has been intense and in several wavebands. Prior to this, these objects were found to be radio sources whose optical appearance was star-like instead of galaxy-like - the first such source to be identified was 3C 48 (Matthews et al., 1961) followed by 3C 196 and 3C 286 (Matthews & Sandage, 1962, 1963). Subsequent to this, absorption lines were detected in the ultraviolet in the quasar spectrum with the first extensive study being of 3C191 (Burbidge & Lynds, 1967). For most quasars, the observed absorption lines could be identified if different lines were interpreted as showing a range of velocity shifts (e.g. Bahcall & Salpeter, 1966) as was demonstrated for the spectral lines from quasar 1116+12 (Bahcall et al., 1966). Thus, the spectral lines observed in absorption with redshifts ranging from close to the emission line redshift to much lower redshifts along the same sightline to a quasar were identified with different species, ionization levels and locations along the line-of-sight to quasars. Intriguingly, several absorption lines could be identified at a common redshift of 1.95 in the spectra of a few quasars (Burbidge & Burbidge, 1967). In fact, Karlsson (1971) suggested that the absorption line redshifts are discretised at an interval of  $\Delta \ln(1+z) = 0.089$  ie detected at redshifts of 0.061, 0.3, 0.6, 0.96, 1.41, 1.96 etc and the effect was stronger in quasars located close to bright galaxies in the sky plane (Karlsson, 1990) - arguing for the spectra to arise within the quasar.

Several early quasar studies suggested that absorption lines were detected in the high redshift quasars especially those with emission line redshifts  $\geq 2$  and that variability was observed in the continuum emission. However as more data accumulated the first inference has not been confirmed whereas the second has been modified to include variability in both continuum and lines. Opinion has been divided between astrophysicists regarding the origin of the absorption spectrum - those who believed that it was intrinsic to the quasar (e.g. Strittmatter et al., 1973; Carswell et al., 1976) and those who believed that it was extrinsic to the quasar ie arising along the sightline (e.g. Bahcall & Spitzer, 1969). How fast the field was evolving and how strong the divided opinion was is evident in comparing the basic premise in a 1976 review article by Strittmatter & Williams (1976) where they favoured an intrinsic origin for the redshifts whereas in a 1981 review article by Weymann et al. (1981) an extrinsic ie cosmological origin for the redshifts was favoured. A hybrid inference was derived by Burbidge & Hoyle (1967) who on finding a comparable number of quasars and radio galaxies in the 3CR catalogue concluded that the two types of objects occupied the same volume of space and hence the high redshifts of quasars were mostly gravitational in origin whereas the low redshifts were cosmological in nature. Schmidt (1969) comments on this hypothesis as being too arbitrary and hence not acceptable. Thus, we find that due to a lack of suitable explanation for the intrinsic cause of redshifts and a disbelief in the gravitational origin kept astronomers from favouring the internal cause. It appeared easier to accept that the range of redshifted lines indicated the different locations of the absorbing gas along the line of sight.

It is now widely accepted by astronomers that the highest redshift emission and absorption lines are intrinsic to quasars whereas the lower redshift absorption lines arise in intervening galaxies/gas. The intervening absorption line systems are believed to be located at velocities offset by  $-3000$  to  $-5000 \text{ km s}^{-1}$  from the emission line velocity. While most astronomers have accepted that quasars are high redshift objects there have also been suggestions that they are local objects, probably ejected from our Galaxy or nearby galaxies and located within 10-100 Mpc (e.g. Terrell, 1966; Hoyle & Burbidge, 1966; Arp, 1974). Terrell (1964) had also inferred, based on the observed variability in quasars, that the emitting region might not be bigger than a few light days in size. It is clear that quasars continue to defy a coherent consistent physical explanation which can encompass its range of observational characteristics. We summarise some of these questions which are explored in this work and explain them in the summary section:

- The spectral lines in absorption in ultraviolet: intrinsic or extrinsic?
- Quasars: local or cosmological?
- The origin of the ultraviolet continuum emission and variability.

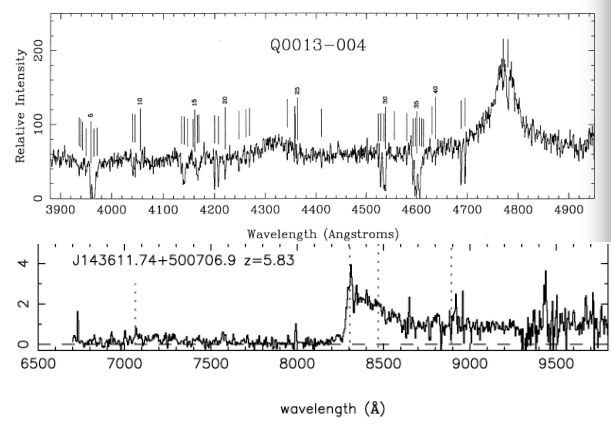


Figure 1: Ultraviolet spectra of quasars Q0013-004 at  $z_{em} = 2.086$  (top) from Sargent et al. (1988a) and of J143611.74+500706.9 at  $z_{em} = 5.83$  (bottom) from Fan et al. (2006). The strong feature in both is the redshifted Lyman  $\alpha$  emission line ( $\lambda_{rest} = 1215.67\text{\AA}$ ) and the absorption features are detected bluewards of the Lyman  $\alpha$  emission line.

- Quasars: galaxies or isolated black holes ?

## 2.1 Emission and absorption line spectra

The observed line spectra towards quasars are complex with high redshift broad/narrow emission lines and several absorption lines detected shortwards of the redshifted Lyman  $\alpha$  emission line (see Figure 1). We refer to the observed emission line redshift by  $z_{em}$  and absorption line redshift by  $z_{abs}$ . Since it is widely accepted that the quasar redshifts are cosmological in origin, the emission lines which are detected at the highest redshift in the spectrum are used to estimate the cosmological redshift i.e.  $z_c = z_{em}$ . The redshifts of active nuclei are preferably estimated from the narrow forbidden emission lines like [OIII] 5007A, [SII] 4068.6A (e.g. Komossa et al., 2008) but since forbidden lines are not detected in all quasars, the broad resonance lines of Mg II in emission are often used. It has been noted that  $z_{em}$  estimated from the broad resonance lines show a velocity offset wrt [OIII] or [SII] lines. For example, high ionization lines like the broad resonance line of C IV shows a blueshifted velocity of  $-564 \text{ km s}^{-1}$  whereas low ionization lines like Mg II show a redshifted velocity of  $161 \text{ km s}^{-1}$  wrt the [OIII] velocity (Vanden Berk et al., 2001). To calibrate this difference, systems where both the forbidden [OIII] lines and broad resonance lines are detected have been used to estimate the velocity offset and the resonance lines in emission have then been used to estimate  $z_c$  for the active nuclei where narrow forbidden lines are not detected (e.g. Tytler & Fan, 1992; Vanden Berk et al., 2001).

Most quasars show a multitude of absorption lines bluewards of the redshifted Lyman  $\alpha$  ( $\lambda_{rest} = 1215.67\text{\AA}$ ) emission line such that  $z_{abs} < z_{em}$ . These absorption lines, many of them doublets, could be identified only if they were detected with different velocity offsets wrt to the quasar redshift. This, then, led to the obvious ques-

tion of whether these velocity shifts which ranged from a few thousand  $\text{kms}^{-1}$  to several tens of thousands of  $\text{kms}^{-1}$  were intrinsic to the quasar or was due to absorption in the gas between us and the quasar. Observations could be interpreted to support either origin but the widely favoured origin is the intervening one probably because no physical reason for such large redshifts arising in the quasar system was convincing enough. The absorption lines which are commonly detected at multiple redshifts in the quasar spectra are doublets of C IV (1548.188Å, 1550.762Å), Si IV (1393.755Å, 1402.770Å), N V (1238.808Å, 1242.796Å) Mg II (2795.528Å, 2802.704Å), triplet of Fe II (2383Å, 2586Å, 2600Å) and the singlets of HI (1215Å), C II (1335Å), Si II (1260Å) and Al II (1671Å). Observations indicate that the C IV doublets are detected in emission and absorption at relatively high redshifts close to  $z_{\text{em}}$  whereas the Mg II doublet is identified in emission close to  $z_{\text{em}}$  and in absorption at much lower redshifts. Neither show significant evolution with redshift (e.g. Sargent et al., 1988b,a; Seyffert et al., 2013; Cooksey et al., 2013; Boksenberg & Sargent, 2015). Mg II lines can arise in gas with a large range in hydrogen column densities -  $10^{17}$  to  $10^{22} \text{ cm}^{-2}$  (Bergeron & Stasińska, 1986).

Table 1: Estimating the intrinsic redshift ( $z_{\text{in}}$ ) from the emission line redshifts ( $z = z_{\text{em}}$ ) of quasars and redshift of the absorption lines of Mg II ( $z_c = z_{\text{MgII}}$ ) using Eqn 1. The sample of 27 quasars is taken from Sargent et al. (1988b).

Quasar	$z = z_{\text{em}}$	$z_c = z_{\text{MgII}}$	$z_{\text{in,em}}$
Q0013-004	2.086	0.4466	1.133
Q0014+818	3.377	1.1109	1.073
Q0058+019	1.959	0.6128	0.835
Q0119-046	1.937	0.6577	0.772
Q0150-203	2.147	0.3892	1.265
Q0207-003	2.849	1.0435	0.883
Q0229+131	2.067	0.3722	1.235
Q0348+061	2.060	0.3997	1.186
Q0440-168	2.679	1.0067	0.833
Q0450-132	2.253	0.4940	1.177
Q0528-250	2.765	0.9441	0.937
Q0837+109	3.326	1.4634	0.756
Q0848+163	1.925	0.5862	0.844
Q0852+197	2.221	0.4151	1.276
Q0958+551	1.751	0.2413	1.216
Q1222+228	2.040	0.6681	0.822
Q1329+412	1.935	0.5009	0.955
Q1331+170	2.084	0.7443	0.768
Q1517+239	1.898	0.7382	0.667
Q1548+093	2.749	0.7703	1.118
Q1623+269	2.526	0.8876	0.868
Q1715+535	1.929	0.3673	1.142
Q2206-199	2.559	0.7520	1.031
Q2342+089	2.784	0.7233	1.196
Q2343+125	2.515	0.7313	1.03
Q2344+125	2.763	1.0465	0.839
Q2145+067	0.990	0.7908	0.112

We recall that the observed redshift of the quasar  $z$ , if

due to multiple reasons, can be written as follows:

$$(1+z) = (1+z_c)(1+z_{\text{in}}); \quad z_{\text{in}} = \frac{1+z}{1+z_c} - 1 \quad (1)$$

$$(1+z_{\text{in}}) = (1+z_D) (1+z_{\text{unknown}}) \quad (2)$$

where  $z_c$  is the cosmological redshift and  $z_{\text{in}}$  is the intrinsic redshift which also consists of two components namely a Doppler shift ( $z_D$ ) and a hitherto unknown ( $z_{\text{unknown}}$ ) component as given in Eqn. 2. In the currently favoured scenario, the intrinsic component consists of only local Doppler shifts which are negligible in comparison to  $z_c$ . Since the cosmological origin of the redshift has been widely accepted but still remains unable to consistently explain several observables, we decided to examine the possibility and origin of the  $z_{\text{unknown}}$  in Eqn 2.

We assume that all the deduced redshifts from an absorption line spectrum of a quasar, except the lowest redshift, include an intrinsic component. In this case, the lowest detected redshift is equal to  $z_c$  of the quasar. The absorption lines of C IV and Mg II are commonly detected in quasar spectra and are generally the highest and lowest redshifted absorption lines respectively. We, thus, started with the assumption that the lowest redshift at which a Mg II absorption line ( $z_{\text{MgII}}$ ) is detected in a quasar spectrum indicates the cosmological redshift  $z_c$  of the quasar i.e.  $z_c = z_{\text{MgII}}$ . Using  $z = z_{\text{em}}$  and  $z_c = z_{\text{MgII}}$  in Eqn 1, we can estimate  $z_{\text{in}}$  for the emission line. If we use  $z = z_{\text{abs}}$  then we can estimate the  $z_{\text{in}}$  for the concerned absorption line (ie other than  $z_{\text{MgII}}$ ). However since  $z_{\text{abs}} < z_{\text{em}}$ ,  $z_{\text{in,abs}} < z_{\text{in,em}}$ . Thus we use  $z = z_{\text{em}}$  to estimate the largest values of  $z_{\text{in}}$  in the quasar.

We used this method on the sample of 27 quasars in Sargent et al. (1988b) and estimated  $z_{\text{in}}$  which are listed in Table 1. If multiple Mg II absorption line redshifts were listed for a quasar, then we used the lowest redshift as  $z_c$ .  $z_{\text{em}}$  ranges from 1.751 to 3.377 for 26/27 quasars and  $z_{\text{MgII}}$  ranges from 0.2413 to 1.46 while the estimated  $z_{\text{in}}$  ranges from 0.667 to 1.276. To show that  $z_{\text{in}}$  is not always largest for the quasar with the largest observed redshift - we draw attention to quasars Q0013-004 and Q0014+818 in Table 1 - Q0013-004 has  $z_{\text{em}} = 2.086$  and  $z_{\text{in}} = 1.133$  while Q0014+818 has  $z_{\text{em}} = 3.377$  while  $z_{\text{in}} = 1.073$ . We were dumbfounded by the remarkable result that  $0.6 < z_{\text{in}} < 1.28$  for 26/27 quasars and were convinced that this result demanded further investigation.

We, then, used the sample of 35629 Mg II absorption lines given in Seyffert et al. (2013) which included multiple redshifted Mg II absorption lines detected towards a quasar. Since we required the lowest redshift at which a Mg II absorption line is detected towards a given quasar, we filtered the samples appropriately and derived a sample of about 25500 quasars for which  $z_{\text{em}}$  ranges from 0.5 to 5 (Figure 2 left) and the range of  $z_{\text{MgII}}$  which is primarily determined by the observing band is from 0.36 to 2.29 (Figure 3). We then repeated the above exercise ie using  $z = z_{\text{em}}$  and  $z_c = z_{\text{MgII}}$  in Eqn 1 to estimate  $z_{\text{in}}$ . The result (Figure 2 right) confirms that  $z_{\text{in}}$  is always  $< 1.25$ . It indicates that the observed limit has to be due to some physical process inside the quasar. The median value of

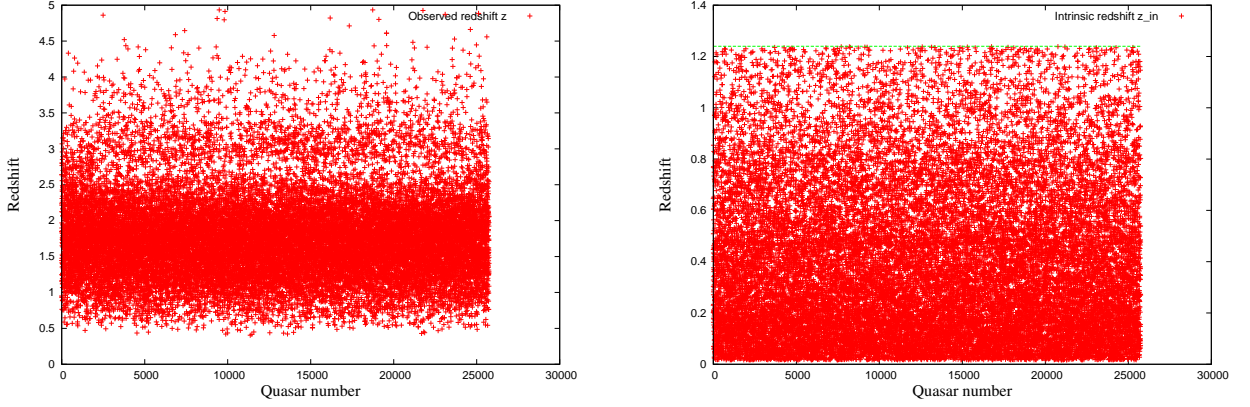


Figure 2: Left panel shows the quasar redshift  $z = z_{em}$  and right panel shows the intrinsic (difference) redshift ( $z_{in}$ ) of the emission line estimated assuming the Mg II absorption detected at the lowest redshift in the quasar spectrum is  $z_c$  using Eqn 1. Each point represents a quasar. The horizontal line in right panel shows the observed cutoff at  $z=1.25$ . The data are taken from the catalog presented by Seyffert et al. (2013).

the distribution is  $z_{in} \sim 0.333$ . If there was no connection between  $z_{em}$  and  $z_{MgII}$  i.e. if the former was  $z_c$  of the quasar and latter was an intervening system, as is generally assumed, then there should have been no limit on  $z_{in}$ . This result, we believe, provides irrefutable evidence to a non-trivial intrinsic component in the observed redshift of quasars and the physical process which gives rise to this component has to be constrained by the result that the maximum value of  $z_{in}$  is 1.25. This value includes contributions from a Doppler effect and an unknown cause as given in Eqn. 2.

From the above results, our reasoning leading to the assumption that  $z_c = z_{MgII}$  where  $z_{MgII}$  refers to the lowest redshift detected in a quasar spectrum is validated. This, then, has very important implications:

1. All the multi-redshifted spectral lines arise inside the quasar system.
2.  $z_c \neq z_{em}$  for a quasar. Instead  $z_c \sim z_{MgII}$  and Figure 3 shows the distribution of  $z_c = z_{MgII}$  of the quasars. The median value of this  $z_c$  distribution is 0.977.
3. The observed range of redshifts in a quasar spectrum are due to an intrinsic physical process such that  $z_{in} < 1.25$  for all lines and the median value of  $z_{in}$  is 0.333.

We, then, used the C IV absorption line catalogue in Cooksey et al. (2013) and estimated the difference between  $z_{em}$  and  $z_{abs,CIV}$  for all C IV line detections along a quasar. The quasar sample is same as the one shown in Figure 2 (left panel) but only those with  $z_{em} > 1.7$  are used in the C IV line analysis. The results are shown in Figure 4. The difference redshifts are  $< 0.185$ . Thus,  $z_{abs,CIV}$  are close to  $z_{em}$  and will also contain a large contribution from  $z_{in}$  which is distinct from  $z_{in,em}$ . This result supports the origin of the C IV lines in the quasar itself otherwise the difference between  $z_{abs,CIV}$  and  $z_{em}$  should

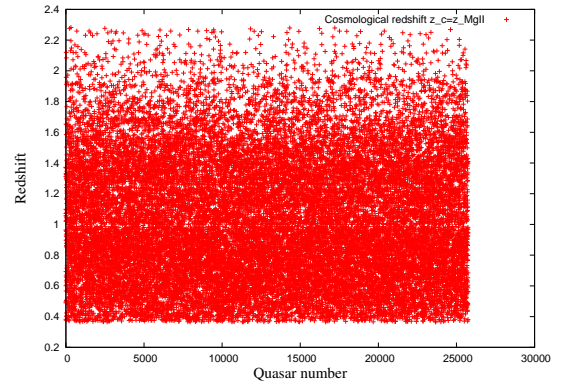


Figure 3: The lowest  $z_{MgII}$  detected towards a quasar for the same sample shown in left panel of Figure 2.  $z_c = z_{MgII}$  as we find from our study. Data taken from the Seyffert et al. (2013) sample.

have been larger and random. Being entirely convinced that the observed redshifts of lines in quasars definitely contain a varying intrinsic component responsible for the multiply-redshifted absorption lines, we examined other observational results in literature with this new perspective. We present some results which are trivially explained with an intrinsic redshift component but often require a contrived explanation for a cosmological redshift:

1. While emission lines are observed in all types of active nuclei, absorption lines at blue-shifted velocities wrt to the emission line are mainly detected towards quasars, a few blazars and Seyfert 1 galaxies. This is a strong argument against the intervening origin for the absorption lines since then the spectra of the nuclei of all distant active galaxies should have detected these. However if the origin of the absorption lines is



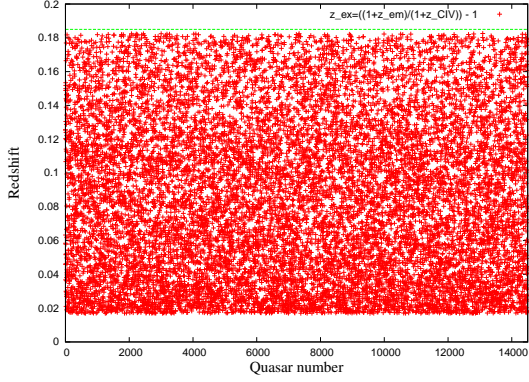


Figure 4: The difference redshift of the emission line and C IV absorption lines towards quasars from Cooksey et al. (2013). The difference redshift  $(z_{em} + 1)/(z_{CIV} + 1) - 1$  is always less than 0.185 shown by the horizontal line.

intrinsic to the quasar then it indicates a difference in the attributes of quasars and other active nuclei.

2. The redshift-magnitude correlation is not followed by quasars unlike active galaxies. This point is explained in the cosmological redshift model as indicating a large spread in the intrinsic luminosities of quasars as compared to other galaxies. We suggest that this correlation is corrupted by the intrinsic redshift component in quasars and should be examined after removing the intrinsic contribution as outlined above.
3. It is believed that the emission lines and the highest redshifted absorption lines in a quasar spectrum are intrinsic to the quasar whereas the rest of the absorption lines arise in the intervening medium. While it is a reasonable assumption, it appears to be fairly adhoc due to lack of better understanding.
4. In a quasar spectrum, the high ionization absorption lines such as C IV and Si IV always appear at relatively higher redshifts compared to the low ionization absorption lines such as Mg II and Fe II. Some of this could be a bias due to the optical observing band. To check the influence of this bias, we plotted both the lines detected in the common redshift range of 1.7 to 2.3 (Figure 5). As seen in Figure 5, a significantly larger number of C IV lines (right panel) are detected compared to Mg II lines (left panel). In fact it appears that C IV lines in this redshift range are detected from most quasars unlike Mg II lines. This result, in the intervening gas model would mean that high ionization systems are more distant than low ionization systems. On the other hand, taking recourse to our inference above wherein all absorption lines arise in the quasar and  $z_{MgII} \sim z_c$ , this result indicates that  $z_c$  of quasars are fairly modest and  $z_{em}$ ,  $z_{abs}$  appear large due to the contribution of  $z_{in}$ . Mg II lines contain a smaller contribution of  $z_{in}$

compared to the C IV lines so that the latter appear at higher redshifts.

5. Boksenberg & Sargent (2015) presented an extensive study of absorption spectra towards nine quasars. Since they believed that the lines arose in the intervening medium whose evolution they were studying, they combined the absorption line data towards all quasars based on the observed redshift. They infer several interesting points based on their comprehensive analysis and we present a few here. Firstly, they find no evolution in any parameter of the CIV systems with redshift although they are detected at the highest redshifts towards quasars. Secondly, they find that the absorption lines with redshift  $\leq 3000 \text{ km s}^{-1}$  offset from the quasar redshift have comparatively harder radiation impinging on them. Thirdly and we think very significantly, Boksenberg & Sargent (2015) find that the column density ratios Si IV/C IV and Si II/C II do not change with redshift whereas the ratios C II/C IV and Si II/Si IV continuously vary with redshift. This is difficult to understand if these lines arise the intervening gas. In an intrinsic origin, this can be understood as different contribution of  $z_{in}$  on the high ionization and low ionization lines so that the ratios of high or low ionization lines will show no evolution with redshift but ratios of high and low ionization species will show a dependence on  $z_{in}$  i.e.  $z$ . We suggest that to study the cosmological variation in these ratios, the  $z_{in}$  component in  $z$  needs to be eliminated.
6. Recently Shen et al. (2016) have studied the dependence of the velocity offset between emission lines of two species and differing ionization on quasar luminosity. Figure 1 in their paper shows their results. The velocity offsets between the narrow forbidden emission lines is small and so is the scatter. This could mean that these lines arise in the same region around the ionizing source. On the other hand, the velocity offsets and scatter between the wide lines are large but similar for He II, C IV and Si IV i.e. these appear to arise in the same region. This is indicative of the different contribution by  $z_{in}$  on the forbidden line velocities and on the wider lines of He II, C IV and Si IV.

Thus, we conclude that both  $z_c$  and  $z_{in}$  make a significant contribution to the observed line velocities in a quasar spectrum and hence influence their overall behaviour. In the following section, we explore the dominant physical process which contributes to the intrinsic redshifts.

## 2.2 $z_{in} \sim z_{\text{unknown}} = z_{\text{gravitational}}(z_g)$

In this section, we search for a physical cause of the intrinsic redshifts in a quasar spectrum which can explain the following:

- $z_{in} < 1.25$ .

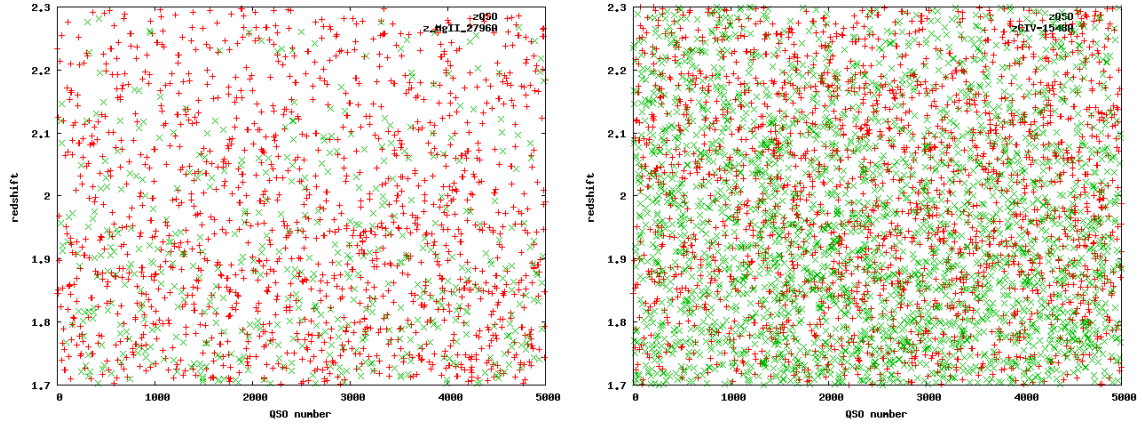


Figure 5: Redshifts of absorption lines of Mg II in green (x; left) and C IV lines in green (x; right) and the emission line redshifts in red (+) in the common redshift range of 1.7 to 2.3. Note the significantly larger number of C IV systems as compared to the Mg II systems at these redshifts. Data on Mg II redshifts from Seyffert et al. (2013) and C IV redshifts from Cooksey et al. (2013) are plotted.

- Large, varying redshifts and line widths of the emission lines and absorption lines.
- No contribution of  $z_{in}$  in the lowest redshift absorption feature due to Mg II.
- The difference between spectra of quasars and other active nuclei especially the absence of absorption lines.

Soon after quasars were discovered, Greenstein & Schmidt (1964) examined the high redshift emission lines detected in the spectra of 3C 48 ( $z_{em} = 0.3675$ ) and 3C 273 ( $z_{em} = 0.1581$ ). Two possible origin scenarios for the high redshift lines were considered (Schmidt, 1963; Greenstein & Schmidt, 1964): (1) cosmological redshifts which was favoured by them and has come to be widely accepted by the astronomical community; (2) gravitational redshifts which was ruled out by them which we recount here. In the gravitational redshift origin suggested by Schmidt (1963), the lines had to arise in a star with a radius of  $\sim 10$  km. On the other hand, the study by Greenstein & Schmidt (1964) found that the gravitational redshift can explain the emission line redshifts if the lines arose in a thin shell of thickness  $10^{-4}$  pc (i.e.  $3 \times 10^{14}$  cm) within a radius of 0.01 pc (i.e.  $3 \times 10^{16}$  cm) around a massive object of mass  $\sim 10^{11} M_{\odot}$ . They ruled out this origin since it was not clear if such massive compact systems could be stable. Interestingly, the authors stated ‘If stable, massive configurations exist, we must re-examine this possibility.’ Moreover, they concluded that if the redshifts were gravitational then the object had to be extragalactic. Hoyle & Fowler (1967) put forward a different model which according to them could give rise to large gravitationally redshifted lines. They suggested that the quasar consisted of a central hot gas cloud which emitted the continuum and spectral lines and which was surrounded by a large number of compact objects like neutrons stars. The compact objects then gravitationally redshifted the emission lines from the central gas cloud as the radiation left the system. Curiously, they could obtain arbitrarily large values

of gravitational redshifts in their model which explained the entire  $z$  of a line. The absorption lines were postulated by them to arise in floating clouds of ions that surrounded the central emitting cloud. The viability of this model has been examined in detail in Das & Narlikar (1975); Das (1979); Zapolsky (1968). The gravitational redshift origin has indeed been considered by several astronomers as a possible cause for the range of absorption line redshifts. It also appears that many of these studies were trying to explain the entire observed redshifts of quasars as being due to a gravitational redshift and hence being stumped. Many observational studies which were not convinced of the gravitational origin, still concluded that the observed redshift contained an intrinsic component (e.g. Burbidge & Burbidge, 1969) but appear to have been unable to find a cause for this as against the cosmological origin. We believe that with much more data on quasars now available for inspection and interpretation, we should be able to conclusively arrive at a physical solution and pave way for future research. We begin by examining gravitational redshift as the  $z_{unknown}$ .

Gravitationally redshifted spectral lines are a natural outcome of the general theory of relativity. As Robert Lawson’s English translation of Einstein’s book (Einstein, 1920) notes ‘An atom absorbs or emits light of a frequency which is dependent on the potential of the gravitational field in which it is situated.’ The shifted frequency of a line emitted in a strong gravitational field was quantified by Einstein to be:

$$\nu = \nu_0 \left(1 + \frac{\phi}{c^2}\right) \quad (3)$$

where  $\nu$  is the observed frequency,  $\nu_0$  is the rest frequency of the spectral line and  $\phi = -GM/R$  is the gravitational potential where  $M$  is the mass of the massive object and  $R$  is the distance of the line forming medium from the massive object. The above equation then gives the expected shifts in the frequency and wavelength of the spectral line

arising in the gravitational potential  $\phi$ :

$$\frac{\nu_0 - \nu}{\nu_0} = \frac{GM}{Rc^2} \text{ or } \frac{\lambda - \lambda_0}{\lambda_0} = \frac{GM}{Rc^2} \quad (4)$$

These are the gravitational redshifts ( $z_g$ ). Einstein noted at that time that it was an open question if such an effect existed. Soon after, Adams (1925) seems to have measured a displacement of about  $23 \text{ kms}^{-1}$  in the velocity of the spectral lines from the white dwarf Sirius B which was attributed to a gravitational redshift. This provided the first evidence of a frequency shift in a line due to the effect of a gravitational potential. The frequency shift caused by the earth's gravitational potential was demonstrated in a neat experiment by Pound & Rebka (1960) and Pound & Snider (1964). More evidence for the existence and detectability of this effect came from the gravitationally redshifted spectral lines detected from several white dwarfs (Greenstein & Trimble, 1967) and absorption lines in the X-ray band from neutron stars showing a gravitational redshift of 0.35 in EXO 0748-676 (Cottam et al., 2002) and a redshift of 0.12-0.23 in 1E 1207.4-5209 (Pavlov et al., 2002). Thus, it is clear that gravitational redshifts are detectable in lines formed near compact objects in our Galaxy and it is reasonable to examine their effect, if any, in the line spectra observed from quasars whose central engine is a supermassive compact object.

Here we revisit the original suggestion in Greenstein & Schmidt (1964) wherein the emission line redshifts of 3C 48 and 3C 273 are due to gravitational redshifts  $z_g$ , if the emission arose in a very thin dense shell located very close to a supermassive black hole in extragalactic systems. We use Eqn 1 to define the observed redshift of the quasar and examine results from the previous section for the possibility of  $z_g$  being the component  $z_{\text{unknown}}$  in  $z_{\text{in}}$  (Eqn. 2).

We start with some physical background on black holes which is relevant for this discussion before we go to the analysis of the redshifted lines. We note that the Schwarzschild radius of an object of mass  $M$  is given by:

$$R_s = \frac{2GM}{c^2} \quad (5)$$

We modify the labels in Eqn 4 and relate the gravitational redshift to the observed velocity shift of the spectral lines  $v$  for connecting to observations:

$$z_g(R) = \frac{(\lambda_{\text{obs}} - \lambda_{\text{rest}})}{\lambda_{\text{rest}}} = \frac{GM}{Rc^2} = \frac{v}{c} \quad (6)$$

Combining Eqns 5,6, we note that a line emitted from  $R \sim R_s$  will show  $z_g \sim 0.5$  when detected by us and  $R$  can be expressed in terms of the Schwarzschild radius  $R_s$  for a given gravitational redshift i.e.

$$z_g(R) = \frac{R_s}{2R} \quad (7)$$

We note that the expression for the gravitational redshift which should be used when  $z_g(R) \rightarrow 1$  is

$$z_g(R) = \frac{1}{\sqrt{1 - \frac{2GM}{Rc^2}}} - 1 \quad (8)$$

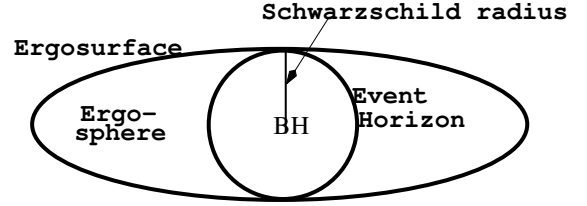


Figure 6: The event horizon and ergosphere of a rotating black hole. For non-rotating black holes, the event horizon and the ergosurface coincide ie a spherical surface with radius  $R_s$ .

and the expression for the cosmological redshift which should be used when  $z_c$  approaches one is

$$z_c = \sqrt{\frac{c+v}{c-v}} - 1 \quad (9)$$

However, for simplicity since we are trying to establish if  $z_{\text{unknown}} = z_g$ , we use the approximations given in Eqn 6 when required.

The event horizon of a black hole is the effective radius of a zone around it from which no information which includes photons can be extracted. Thus, the event horizon defines the black hole extent. In case of non-rotating black holes also known as Schwarzschild black holes, the extent of the event horizon is defined by the Schwarzschild radius  $R_s$  (see Figure 6). Thus, if the spectral lines are formed just outside the event horizon, they will be detected with a gravitational redshift of 0.5 and this is the maximum redshift that the gravitational potential of a non-rotating black hole can introduce in the spectral lines. In case of a rotating black hole also known as a Kerr black hole, the event horizon is smaller than the Schwarzschild radius in the non-polar regions. It is  $R_s/2$  at the equator for a maximally rotating black hole. There exists a region between the event horizon and the Schwarzschild radius in rotating black holes which is referred to as the ergosphere. The ergosphere has a peculiar egg-shaped structure (see Figure 6) since it arises due to a modification in the gravitational field of the black hole due to its rotation. The rotation is maximum in the equatorial zones so the extent of the ergosphere is largest there and rotation is zero at the poles where the event horizon coincides with  $R_s$  and there is no ergosphere (see Figure 6). In such a black hole, a spectral line formed near the event horizon in the equatorial regions can be detected with a maximum gravitational redshift close to one whereas a spectral line formed in the polar regions can only suffer a maximum  $z_g$  of 0.5. To summarise, a non-rotating Schwarzschild black hole can explain upto  $z_g \sim 0.5$  while a rotating Kerr black hole can explain upto  $z_g \sim 1$  i.e. the maximum allowed  $z_g$  for any black hole configuration is one.

We show the gravitational redshifts suffered by spectral lines arising at different distances from the black hole in the top panel of Figure 7. In the lower panel, we show  $R_s$  for black holes of different masses. Thus, the Schwarzschild



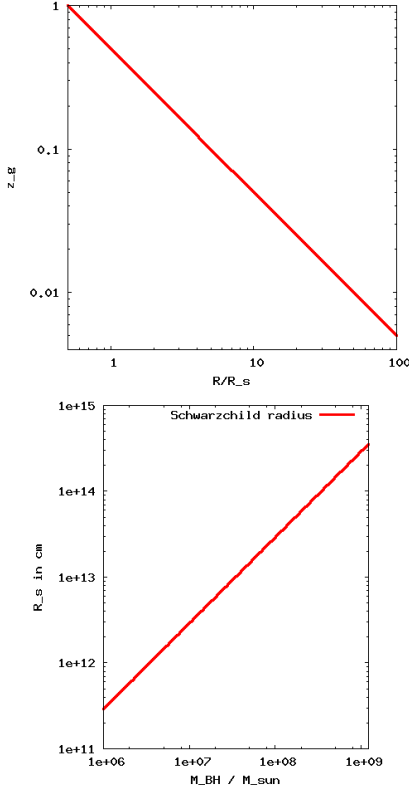


Figure 7: Top panel shows the gravitational redshift that a line will suffer when formed at different distances from the black hole. The second panel shows the Schwarzschild radius in physical units for different black hole masses.

radius of a black hole of mass  $10^9 M_\odot$  is  $3 \times 10^{14}$  cm while that of mass  $10^6 M_\odot$  is  $3 \times 10^{11}$  cm. However as evident from Figure 7 (top), the effect of the gravitational potential of the black hole felt by the line forming gas, if located near  $R_s$  will be the same in both cases. In other words, the gravitational redshift can be used to estimate the ratio  $M_{BH}/R$  but other observational results are required to estimate  $M_{BH}$ .

Equipped with this background on black holes, we find that the result we obtained in the previous section that  $z_{in} < 1.25$  for all quasars assuming  $z_c = z_{MgII}$  is extremely significant and conclusive when considered with two other details - (1) the largest value of  $z_g$  is one and (2)  $z_{in}$  consists of  $z_D$  and  $z_{unknown}$  (Eqn 2). If we assume that  $z_{unknown} = z_g$  then substituting the maximum value of  $z_g$  and  $z_{in} = 1.25$  in Eqn 2 gives  $z_D = 0.12$  i.e. the contribution of Doppler velocity component is  $\leq 36000 \text{ km s}^{-1}$ . This component will be different for different quasars but will be similar for the spectral lines detected from a quasar unlike  $z_g(R)$  which changes for lines which form at different  $R$  from the black hole in the same quasar.  $z_D$  can be due to incorrect  $z_{MgII}$  which introduces an offset in  $z_c$  and/or due to outflow/inflow in the line forming region.  $z_D$  makes a small contribution to  $z$  and we are not concerned with it here. The spectral lines from quasars in a 25500 large sample include contribution from  $z_{unknown} = z_g \leq 1$  and a small component  $z_D < 0.12$ . We thus conclude that the limit  $z_{in} < 1.25$  is mainly dictated

Table 2: The estimated values of cosmological component of redshift ( $z_c$ ) for different observed redshifts ( $z$ ) after removing  $z_{in} \sim z_g = 1$  in Eqn 1 are listed here.

$z = z_{\text{emission}}$	$z_{\text{cosmological}}$
7	3
6	2.5
5	2
4	1.5
3	1
2	0.5

by the limit  $z_g \leq 1$  imposed by black hole physics. Since  $z_g(R)$  varies as a function of  $R$ , this explanation trivially explains the range of redshifted lines observed in a quasar spectrum as lines that arise at different  $R$ . This, then, leads to the inevitable and clear conclusion that the large observed spectral line redshifts and the large range in absorption line redshifts in a quasar spectrum are a result of the varying gravitational potential experienced by the line photons arising in gas located at different distances from the black hole.

This discussion then leads us to the following important inferences:

- For quasars,  $z_{unknown} = z_g$  and  $z_c \leq 3$ . The large observed redshifts  $z$  are because of the contribution of  $z_g$ . The  $z_c$  estimated after removing  $z_g$  from  $z$  are listed in Table 2.
- $z_g \leq 1$  is the major component of  $z_{in}$  and hence leads to the limit  $z_{in} < 1.25$  in quasars.
- Now that we know that lines are shifted by  $1 < z_g < 0.5$ , this proves that rotating black holes exist and contain matter within their ergosphere.
- The emitting zone is located closer whereas absorption zones are further from the black hole and hence lines appear at different redshifts.

We note that the explanation presented above violates no black hole physics nor does it demand any ‘new’ physics. In fact, it is heartening to note that all the required physics has been known for a long time. There are obviously several questions which need to be addressed now that it is clear that the quasar spectrum is intrinsic and the range of redshifts are due to the gravitational potential of the black hole.

After finding a satisfactory explanation for the redshifted quasar spectra, we decided to estimate the  $z_g(R)$  of the absorption lines for a few quasars. In the remaining discussion, we refer to  $z_{in}$  as  $z_g$  but with the clear understanding that  $z_g$  can only take values upto one and if  $z_{in}$  is greater than one then it definitely includes a contribution from  $z_D$ . By the same token, we are aware that for  $z_{in} < 1$  there will be a contribution from  $z_D$  but this is difficult to estimate here and hence, for simplicity, we assume that  $z_{in} = z_g$  when  $z_{in} < 1$ . The  $z_g(R)$  of the multiple C IV absorption lines detected towards six quasars

Table 3: The gravitational redshifts estimated for the multiple absorption lines of C IV 1548A detected at different redshifts ( $z_{\text{CIV},\text{abs}}$ ) in the spectra of six quasars.

$z_{\text{CIV},\text{abs}}$	$z_{\text{in}} \sim z_{\text{g,CIV},\text{abs}}$
Q0848+163 <sup>1</sup>	
$z_{\text{em}} = 1.925, z_{\text{MgII}} = 0.5862, z_{\text{g,em}} = 0.844$	
1.4575	0.5493
1.4684	0.5562
1.4704	0.5574
1.9159	0.8383
Q0014+818 <sup>1</sup>	
$z_{\text{em}} = 3.377, z_{\text{MgII}} = 1.1109, z_{\text{g,em}} = 1.073$	
2.4932	0.6548
2.7980	0.7992
2.8004	0.8004
3.2265	1.0022
Q0837+109 <sup>1</sup>	
$z_{\text{em}} = 3.326, z_{\text{MgII}} = 1.4634, z_{\text{g,em}} = 0.7561$	
2.4165	0.3869
2.9558	0.6058
3.1428	0.6817
54452-2824-554 <sup>2</sup>	
$z_{\text{em}} = 2.5566, z_{\text{MgII}} = 2.08431, z_{\text{g,em}} = 0.1531$	
2.08788	0.0011
2.14618	0.0200
2.21361	0.0419
2.38185	0.0965
52178-0702-503 <sup>2</sup>	
$z_{\text{em}} = 2.6929, z_{\text{MgII}} = 0.83151, z_{\text{g,em}} = 1.0163$	
2.16934	0.7305
2.18427	0.7386
2.22892	0.7629
2.52017	0.9220
52618-1059-146 <sup>2</sup>	
$z_{\text{em}} = 4.1541, z_{\text{MgII}} = 2.07092, z_{\text{g,em}} = 0.6783$	
3.42263	0.4402
3.53558	0.4769
3.73894	0.5432

<sup>1</sup>  $z_{\text{MgII}}$  from Sargent et al. (1988b) and  $z_{\text{CIV}}$  from Sargent et al. (1988a)

<sup>2</sup>  $z_{\text{MgII}}$  from Seyffert et al. (2013) and  $z_{\text{CIV}}$  from Cooksey et al. (2013).

were estimated using the same method we used for emission lines ie  $z = z_{\text{abs}}$  and  $z_c = z_{\text{MgII}}$  in Eqn 1. These are listed in Table 3. Three quasars which had data on both Mg II and several C IV lines were selected from Sargent et al. (1988b,a) and another three from the catalogues by Seyffert et al. (2013) and Cooksey et al. (2013). As seen in Table 3, C IV absorption lines are detected at a number of redshifts towards the same quasar due to different  $z_g(R)$  estimated in the second column of Table 3. In other words, the absorption lines arise in multiple zones located at different radial separations from the event horizon. For example, the result on Q0014+818 with  $z_{\text{em}} = 3.377$  where the  $z_g(R)$  for the four different C IV absorption features vary from 1.0022 to 0.6548 can be interpreted as lines arising in multiple absorbing zones distributed from very close to the event horizon i.e.  $R_s/2$  to  $R_s$  in a rotating black hole as shown in top panel of Figure 8. On the other hand, in quasar 52618-1059-146 with  $z_{\text{em}} = 4.1541$ , the  $z_g(R)$  of all the C IV absorption features are close to 0.5 indicating absorbing zones near  $R_s$  as shown in bottom panel of Figure 8. These examples demonstrate that the quasar population at all cosmological redshifts show a large range in  $z_g(R)$ . As seen in Figure 8, if  $M_{\text{BH}} = 10^9 M_\odot$  then the C IV absorbing zone is located between  $1.5 \times 10^{14}$  cm to  $4 \times 10^{14}$  cm in the quasars plotted in the top panel and between  $1.5 \times 10^{14}$  cm and  $2 \times 10^{17}$  cm in the quasars plotted in the lower panel. Note that  $R_s = 3 \times 10^{14}$  cm for a black hole of mass  $10^9 M_\odot$ .

The widths of the spectral lines arising so close to the black hole will be dominated by the varying gravitational potential in the line forming zone and hence cannot be used to estimate  $M_{\text{BH}}$ . Instead, it can be used to estimate the fractional line-of-sight extent  $\Delta R/R$  of the line forming region as given by Greenstein & Schmidt (1964):

$$\frac{\Delta R}{R} = \frac{\Delta \omega}{\lambda_{\text{obs}} - \lambda_{\text{rest}}} \quad (10)$$

where  $R$  is the radial separation of the region from the black hole and  $\Delta \omega$  is the observed line width. For example, the C IV 1548A line which shows a gravitational redshift of 0.5 will arise at a distance of  $3 \times 10^{14}$  cm if we assume the black hole has a mass of  $10^9 M_\odot$ . If the observed linewidth is 50 Å, then it can be surmised that the region has an extent of  $0.2 \times 10^{14}$  cm. This C IV line will appear at a wavelength of 2322 Å. We show how the observed C IV 1548 Å line width gives input into the fractional thickness of the line forming region  $\Delta R/R$  for gravitational redshifts of 0.5 and 1 in Figure 9. As the observed line width increases, the fractional thickness of the line forming region increases. Thus we find that  $z_g$  is determined from the observed line wavelength,  $M/R$  is determined from  $z_g$  and  $\Delta R/R$  can be determined from the observed line width. However further independent information is required to determine  $M_{\text{BH}}$  and hence  $R$  and  $\Delta R$ .

In the previous section, we have already demonstrated how an intrinsic origin of the line spectrum in quasars can explain several observational results. Here we show how  $z_{\text{in}} \sim z_g$  further simplifies the explanations. We start with

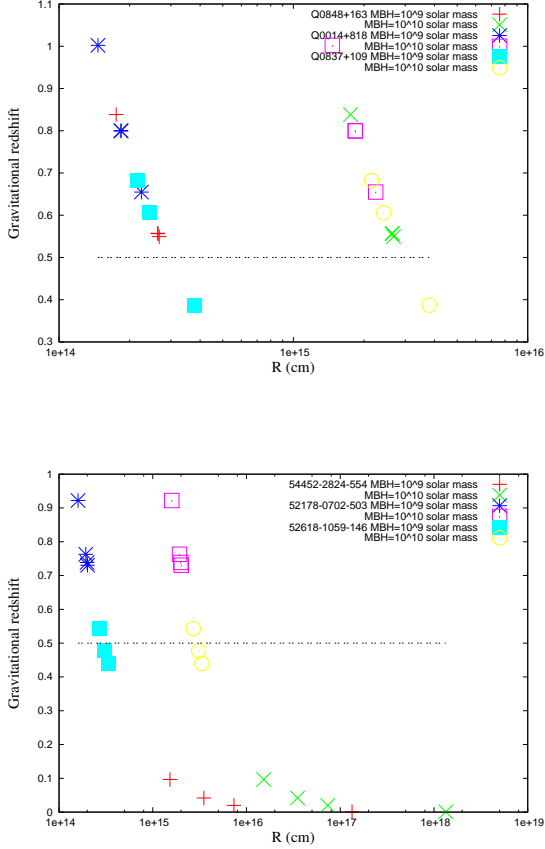


Figure 8: The estimated  $z_g$  for C IV absorption lines listed in Table 3 and the implied distances of the line forming region from black holes of masses  $10^8$  and  $10^9 M_\odot$  are shown in both the panels. The dashed line is drawn at  $z_g = 0.5$  and the intersection with the data points indicate the Schwarzschild radius of that black hole mass. All points above this line require the absorbing gas to be located inside the ergosphere.

the six points listed in section 2.1:

- Point 1 was already explained by an intrinsic origin. In the gravitational origin, it indicates differences in the distribution of matter around the black hole and their physical conditions. Point 2 - the observed quasar redshift as concluded here, has a non-cosmological gravitational component which needs to be removed before the magnitude-redshift correlation can be studied. Point 3 is no longer an issue since all the spectral lines arise in the quasar system and no adhoc classification is needed.
- Point 4 - the high ionization lines appear at higher redshifts for all quasars indicating they are formed closer to the black hole where the gravitational potential is deeper and the radiation field is stronger. The low ionization lines arise farther away from the black hole at lower redshifts (ie potential) and in a weaker softer radiation field.
- The explanation for Point 5,6 is similar to point 4.

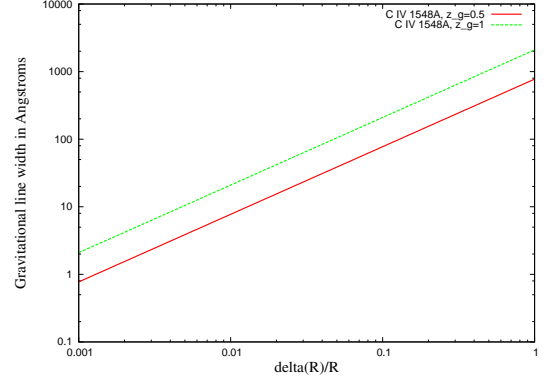


Figure 9: The variation in the observed line width of the C IV 1548A line as a function of  $\Delta R/R$  for  $z_g = 0.5$  (red, solid) and  $z_g = 1$  (green, dashed) are shown.

The dependence of column density ratios on redshifts in a quasar spectrum is actually a dependence on the gravitational component of the redshift. If the high ionization lines of C IV and Si IV arise in the same region closer to the black hole then the ratio C IV/Si IV will not show any dependence on redshift (Boksenberg & Sargent, 2015) since both lines have same contribution from  $z_g$ . The same argument holds for C II and Si II. However when the ratios of differing ionization species are considered ie C II/C IV and Si II/Si IV, then since C II (and Si II) and C IV (and Si IV) arise in different absorbing zones around the black hole, they are shifted by different  $z_g$  and hence appear to show a variation with  $z$ . In fact, results presented in Shen et al. (2016) also give evidence to the forbidden lines arising in a common region and showing the same  $z_g$  and He II, C IV and Si IV arising in another common zone and showing the same  $z_g$ . This then indicates segregation of line forming zones around the quasar based on densities and incident radiation field and can be used to understand the quasar structure.

- Quasars at  $z \sim 6$ . It is observed that the Gunn-Peterson trough (Gunn & Peterson, 1965) becomes more prominent with increasing redshift of a quasar, so that most quasars near  $z \sim 6$  show the trough. However significant differences are noted in spectra of quasars with the same observed redshift (e.g. Fan et al., 2006) making it difficult for cosmological models to explain the result. In the gravitational redshift model, the highest redshift quasars contain large contributions from both  $z_g$  and  $z_c$ . So if  $z_g \sim 1$  for a  $z = 6$  quasar, then its cosmological redshift is only  $z_c = 2.5$  as listed in Table 2! It would be interesting to confirm this by searching for Mg II absorption near redshift 2.5 along the sightlines to quasars with redshift near 6. In this case, the Gunn-Peterson trough is due to the joint effect of broad overlapping lines

and coarse spectral resolution and has no connection to the universe at  $z_c \sim 6$ .

- It has been observed that the number of absorption features detected in spectra of quasars at high redshifts are not an extrapolation from lower redshifts (e.g. Schneider et al., 1991). Such a correlation is expected in the intervening origin for the absorbing gas and the lack of correlation has baffled astronomers. However, we note that no such correlation is expected in a gravitational origin. Instead the absorption features depend on the distribution of matter around the black hole.

Thus it is clear that the contribution of  $z_g \leq 1$  is responsible for several interesting redshift characteristics observed in a quasar spectrum.

### 2.3 Ultraviolet continuum

Quasars generally show strong ultraviolet continuum emission (see Figure 10) often referred to as the ‘blue’ bump and which appears to be similar to the uv upturn (part of the blue bump) widely observed in the nuclei of elliptical galaxies and spiral bulges. IUE data suggested that the continuum emission of quasars showed excess in the ultraviolet (e.g. Bergeron & Kunth, 1983). The thermal component of the continuum emission is believed to arise in the accretion disk around the black hole, modelled to fit the observed spectra of quasars and Seyfert galaxies (e.g. Sun & Malkan, 1989). Since the quasar ultraviolet continuum is often corrupted by the presence of numerous spectral lines, we also examined studies of the upturned ultraviolet spectra of the nuclei of elliptical galaxies. The assumption is that the basic physics behind the quasar continuum in the ultraviolet should be applicable to all active nuclei which is reasonable since most seem to show the blue excess. Thus, in the following we discuss the ultraviolet continuum from quasars and nuclei of galaxies.

The spectra taken by the International Ultraviolet Explorer (IUE), launched in 1978, of quiescent and active population of early type galaxies showed a rise in the blue/ultraviolet emission shortwards of 1550 Å which appeared to be absent in star forming galaxies (Bertola et al., 1987). Interestingly, it was found that this ultraviolet upturn was a nuclear phenomenon which got diluted when the signal of the entire galaxy was included (Bica et al., 1996). Moreover the nuclear spectra of some of these galaxies showed dips near 1400 Å and 1600 Å (Bica et al., 1996). The ultraviolet upturn was intriguingly similar to the excess recorded in the spectra of subdwarf stars with temperatures 110000-150000K or of hot DO type white dwarfs with temperature  $> 75000$  K or of nuclei of planetary nebulae and the the absorption dips near 1400Å and 1600Å were similar to those seen in DA4 or DA5 white dwarfs which have temperatures of 12000-20000 K (Bica et al., 1996). This prompted Bica et al. (1996) to conclude that the ultraviolet upturn could indicate the presence of such stellar objects in the central region of the galaxies. We recall that Matthews & Sandage (1963) had noted a

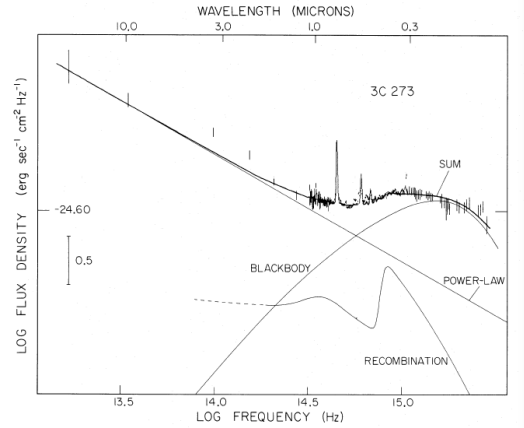


Figure 10: The continuum emission of quasar 3C273 at  $z_{em} = 0.158$  is shown from ultraviolet to infrared. Similar spectra are observed from other active nuclei also. Note the blue ‘bump’ in the ultraviolet and the three components which are required to fit the spectrum. Figure is copied from Malkan & Sargent (1982).

similarity between the colours of old novae/white dwarfs and quasars (3C 48, 3C 196, 3C 286). This was supported by Burbidge et al. (1967) who commented on the similarities in the absorption spectra of the white dwarf Hz 29 (Greenstein & Matthews, 1957) and quasars. Malkan & Sargent (1982) found that the observed continuum spectra from infrared to ultraviolet of several quasars and Seyfert 1 galaxies could be explained by the combination spectrum of (1) a power law of index  $-1.1$  (2) optically thin Balmer continuum emission (3) single temperature black body emission from gas with temperatures between 20000 and 30000 K as shown in Figure 10. For comparison, we show the spectrum of the white dwarf VW Hyi from near-infrared to ultraviolet wavelengths (Mateo & Szkody, 1984) in Figure 11. The similarity is unmistakable in that the continuum starts rising at the near-ultraviolet wavelengths (note that the scales are different) and a separate thermal component has to be included in the model to explain the observed ultraviolet emission. This indicates that both white dwarfs and quasars have a black body component which dominates the continuum emission at ultraviolet wavelengths.

Another similarity to quasars is observed in the absorption features detected in the ultraviolet spectra of white dwarfs (e.g. Greenstein & Matthews, 1957; Dupree & Raymond, 1983; Bannister et al., 2003). IUE detected narrow absorption lines of highly ionized ions such as C IV, Si IV with a range of systemic velocities in the white dwarf spectra (e.g. Dupree & Raymond, 1983) indicating that such highly ionized species exist in the immediate vicinity of the white dwarf. Bannister et al. (2003) studied 23 hot white dwarfs and detected absorption lines of CIV and also found that these lines were blue-shifted from the photospheric line velocities. Holberg et al. (1998) studied 55 white dwarfs and separated the absorption lines forming in the photosphere, circumstellar material and in the interstellar medium and inferred that several lines were blue

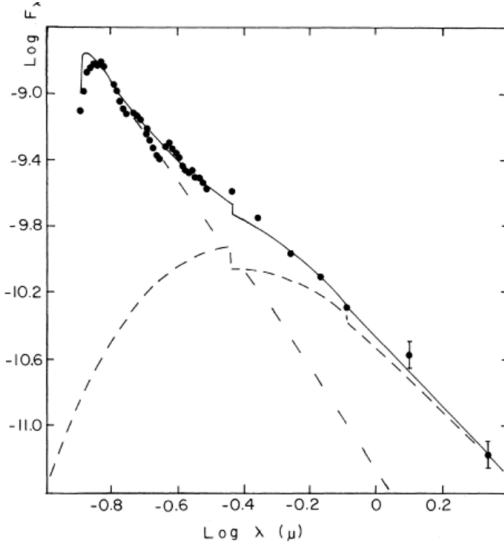


Figure 11: The continuum emission spectrum of the white dwarf VW Hyi from ultraviolet to near-infrared. The long dashed line shows the spectrum of a 20000 K stellar atmosphere and short dashed line represents an accretion disk. Figure is copied from Mateo & Szkody (1984).

shifted from the photospheric velocities. These lines, interestingly, were always detected at a blue shifted velocity wrt to the photospheric velocities and distinct from the interstellar medium velocities. A possible origin for the blue-shifts wrt to the photospheric velocities could be the reducing effect of the gravitational potential of the white dwarf as the line forms at an increasing distance from the white dwarf. The velocity shifts due to the gravitational potential have been estimated to be  $25 - 80 \text{ km s}^{-1}$  depending on the mass of the white dwarf and its composition (Greenstein & Trimble, 1967, Figure 3 in the paper). Mateo & Szkody (1984) reported a wide Lyman  $\alpha$  absorption feature in the spectrum of the white dwarf VW Hyi. Panek & Holm (1984) also reported the detection of a broad Lyman  $\alpha$  absorption with wings (similar to a damped Lyman  $\alpha$  feature in a quasar spectrum) and Mg II lines in emission in the spectrum of the dwarf nova U Gem. We recall that a classical nova is formed in a binary system consisting of a white dwarf and a main sequence or red giant companion star when accreted mass on the white dwarf ignites in an explosive thermonuclear reaction once it crosses a certain density and temperature. The nova explosion is detectable at wavelengths ranging from  $\gamma$  rays to radio.

The observational similarities in the ultraviolet between white dwarfs and quasars are many. They share a similar continuum emission spectral shape. They both show gravitationally redshifted absorption lines of highly ionized species and a broad Lyman  $\alpha$  absorption. All these suggest that quasars share some physical properties with white dwarfs. In the next subsection we use these important clues to gain further insight into quasars.

### 2.3.1 Hot degenerate matter surface

We infer from the above discussion that the ultraviolet continuum in quasars can be explained by radiation from a black body with temperatures ranging from 10000 to 150000 K.

We recall that once a low mass star exhausts the fuel in its core, thermonuclear reactions stop and the star starts collapsing under gravity. It is estimated that when the densities are around  $10^5 - 10^8 \text{ gm cm}^{-3}$ , the electron degeneracy pressure can balance the gravity of the low mass star and a white dwarf is formed. If the star is massive but less than about  $8 M_{\odot}$ , then the phase of contraction after the fuel in its core is exhausted will stop only when the densities exceed the nuclear densities i.e.  $> 1.2 \times 10^7 \text{ gm cm}^{-3}$  and neutron degeneracy pressure halts the gravitational collapse. In fact, the densities in neutron stars can get as high as  $10^{16} - 10^{17} \text{ gm cm}^{-3}$  (Shapiro & Teukolsky, 1983).

Keeping this in mind, we shift the discussion to quasars. It is accepted that the central object in a quasar is a supermassive black hole. The black hole will accrete matter and it is reasonable to expect the density of the matter to increase as it falls towards the black hole. The infalling matter, at some distance from the black hole, can accumulate with densities  $> 10^8 \text{ gm cm}^{-3}$  leading to degenerate neutron matter collecting around the black hole and at some point, being supported against further gravitational collapse by neutron degeneracy pressure. Thus, it appears reasonable to postulate that a degenerate neutron surface forms and exists in equilibrium around the black hole. The immense gravity of the black hole can heat up this surface to high temperatures and it can possibly emit in X-rays. Outside this degenerate neutron surface, the matter will have lower densities but once matter accumulates at densities  $10^5 - 10^8 \text{ gm cm}^{-3}$  then the electron degeneracy pressure can counter the strong gravity of the black hole and the degenerate matter can remain in equilibrium. This, then, forms a degenerate electron shell outwards of the neutron shell. Again the immense gravitational energy of the black hole can cause this surface to be heated up to high temperatures and radiate ultraviolet continuum like a white dwarf surface. Outwards of this could be lower density non-degenerate matter which contributes to the line spectrum. In fact, this appears to be the most logical setup of matter around any black hole.

Thus, the ultraviolet continuum observed in quasars will be emission from the degenerate matter surface around the black hole. Since there are quasars which are X-ray bright and others which are ultraviolet-bright: it needs to be investigated if these can be interpreted as evidence to the type of degenerate matter surface which dominates the continuum emission of a particular quasar. While it appears most reasonable to expect both a degenerate neutron and electron surface around a black hole - there might exist a variety which needs to be examined from observations and physical understanding of degenerate matter.



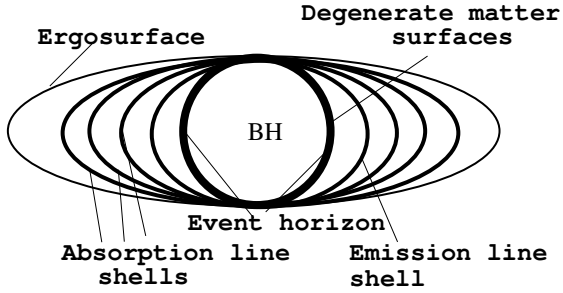


Figure 12: Proposed structure of a quasar. The dense degenerate matter shells, line emitting shell and absorbing shells are all located inside the ergosphere of a rotating black hole. The spectral lines arising in matter inside the ergosphere will suffer a redshift ranging from  $\sim 1$  (close to event horizon) to 0.5 (close to the ergosurface) due to the strong gravitational potential of the black hole (BH).

### 3 Proposed structure of a quasar

Amazingly, it appears that the discussion so far has uniquely determined the structure of a quasar which is schematically shown in Figure 12 and described below.

A supermassive black hole is the central object. Matter is being accreted by the black hole and compressed to progressively larger densities as it approaches the black hole. At appropriate matter densities, the degeneracy pressure of neutrons and electrons will be sufficient to support the matter from further gravitational collapse. Thus, in the quasar structure, the black hole is surrounded by a shell of matter supported by degenerate neutron pressure and outside that a shell supported by degenerate electron pressure. As mentioned in the previous section, the degenerate neutron shell can have densities upto  $10^{17} \text{ gm cm}^{-3}$  while the degenerate electron shell can have densities upto  $10^8 \text{ gm cm}^{-3}$ . The matter outside the degenerate shells will be non-degenerate and will accumulate in dense shells with densities  $\leq 10^5 \text{ gm cm}^{-3}$ . The hot degenerate electron shell will give rise to an intense ultraviolet continuum which bears close resemblance to the white dwarf continuum. Its hard radiation field will ionize and heat a Stromgren shell (?) around it where several elements including hydrogen will emit spectral lines. Since some quasars show the existence of forbidden emission lines which will collisionally deexcite if densities  $> 10^8 \text{ cm}^{-3}$ , we suggest that there should exist a relatively lower density ( $< 10^8 \text{ cm}^{-3}$ ) region around the degenerate matter shells in some quasars where the forbidden lines can arise and which could have an origin similar to the stellar cavities seen around stars. Surrounding this ‘cavity’ would then be the dense ionized shell which emits Lyman  $\alpha$  and resonance lines of highly ionized species such as C IV, Si IV. We note that the forbidden lines can also arise in small lower density pockets located inside the Stromgren shell. Since the emission lines arise in the shell located closest to the black hole and are formed under the influence of the

strongest possible gravitational potential, their velocities contain the largest contribution from  $z_g(R)$  in the spectrum. Outwards of this ionized Stromgren shell, matter will accumulate to form cooler dense shells which will absorb the ultraviolet continuum from the hot degenerate matter surface and give rise to the absorption line spectrum. The matter at different distances from the black hole will absorb different wavelengths and give rise to the observed absorption line spectrum of the quasar. Matter is highly ionized in the shells closest to the emission line shell as can be surmised from the highly ionized species such as C IV and Si IV which are detected in absorption at redshifts which are closest to the emission line redshifts (see Figure 4). Such absorbing shells will continue forming as matter is accreted. The spectral lines will keep appearing at decreasing redshift as compared to the emission lines as they arise in radially distant shells as long as they lie within detectable influence of the gravitational potential of the black hole. The absorption lines which arise far from the black hole and hence are not shifted by the gravitational potential, can then give an estimate of the  $z_c$  of the quasar as we had assumed in  $z_c = z_{MgII}$ . The emission and absorption lines which show  $z_g > 0.5$ , have to arise from matter inside the ergosphere of a rotating black hole. The distinct geometry of the ergosphere (see Figure 12) can be assumed by the equipotential shells which can lend the appearance of a thick accretion disk to the continuum emitting and line forming regions. Any emitting/absorbing shells in the polar regions of the black hole will necessarily have to be outside the ergosphere since the ergosurface and the event horizon coincide in the polar regions. Thus, in this structure, lines formed in the equatorial plane of a rotating black hole can suffer a maximum gravitational redshift of 1 whereas those formed in the polar regions can only suffer a maximum gravitational redshift of 0.5 which is also the maximum gravitational redshift that can result from a non-rotating black hole.

This structure, we note, can satisfactorily explain the ultraviolet observations of quasars - both continuum and spectral lines within the ambit of black hole physics. It also explains the similarities noted between the ultraviolet properties of quasars and white dwarfs such as the blue bump and gravitationally redshifted absorption lines of highly ionized ions C IV and Si IV. The large gravitational field of the black hole can amplify the luminosity of the quasar since the emission from the event horizon of a black hole is expected to be boosted by a staggering factor of  $\sim 10^{27}$  (Shapiro & Teukolsky, 1983). The details of this needs to be studied but since the degenerate matter shells are expected to be located just outside the event horizon, an obvious inference would be that such boosting is responsible for the large luminosities of quasars. This structure for a quasar naturally emerges from the observational results and hence successfully accounts for quasar observables making it the most plausible model of a quasar.

### 3.1 Other active nuclei

In this section, we discuss blazars and Seyfert 1 nuclei and comment on their structure. A few blazars and Seyfert 1 galaxies show the presence of absorption features detected bluewards of the emission lines in their spectra while broad emission lines are observed in Seyfert 1 and some blazars and radio galaxies.

#### 3.1.1 Blazars

Blazars are classified into BL Lac objects and flat spectrum radio quasars (FSRQs). BL Lacs occasionally show line features superimposed on a mostly featureless flat continuum spectrum. BL Lacs are radio-loud, highly variable and show a stellar-like appearance in the optical. In fact, BL Lacs are believed to be radio quasars observed along the radio jet or minor axis. The FSRQs are generally more energetic and show wide emission lines in their spectra. Here we estimate the intrinsic redshifts shown by the emission lines from BL Lac and FSRQ objects using the method outlined earlier.

We use the sample of 23 BL Lac objects given in Bergeron et al. (2011) for which Mg II absorption lines have been recorded to estimate the maximum gravitational redshift in the spectrum (see Table 4). We notice that BL Lacs show a lower observed redshift range (0.875 to 1.522) compared to quasars although the range of  $z_{\text{MgII}}$  (0.2527 to 1.2847) seems comparable (also see Table 1). Since  $z_{\text{MgII}}$  is a proxy for  $z_c$ , this means that quasars and BL Lacs have similar cosmological redshift distribution and the difference in the observed redshifts is due to the different contributions of  $z_g$  to the line velocities. We find the remarkable result that 22/23 BL Lacs show  $z_g < 0.5$  as listed in Table 4 ( $z_g$  ranges from 0.017 to 0.49). *Clearly the spectral lines in BL Lacs, when detectable, arise in a lower gravitational potential compared to quasars.* This, we believe, is highly significant and should be verified on a larger sample. It gives independent support to the existing model of a polar sightline defining a BL Lac. Since at the poles the ergosphere coincides with the event horizon for all black holes,  $z_g \leq 0.5$  for any line arising there. The other explanation can be that the black hole in BL Lacs are non-rotating and hence  $z_g \leq 0.5$ . We recall that BL Lacs generally show a flat spectrum with few spectral lines. This can be explained if the equipotential degenerate matter and line forming shells are located inside the ergosphere and hence not detectable when viewed from the poles. If BL Lacs contained a non-rotating black hole then the degenerate matter and line forming shells can be arranged as spherical equipotential shells around the event horizon and we should have detected numerous spectral lines in their spectrum since orientation would play no role in the nature of the observed spectra. We end by inferring that BL Lacs are quasars with a rotating black hole viewed polewards and hence the maximum  $z_g$  shown by spectral lines is 0.5. We note that this supports the inference derived from radio observations.

We also used the same method on a sample of 75 FSRQs with available Mg II absorption line redshifts (Chand &

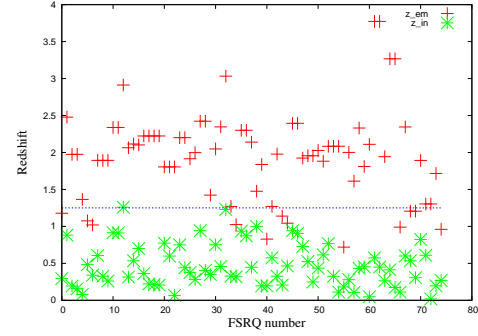


Figure 13: The observed redshift  $z$  (in red +) and intrinsic redshift  $z_{in} \sim z_g$  (in green \*) estimated from  $z_{\text{MgII}}$  for FSRQ are shown. The horizontal line is drawn at redshift=1.25. The data has been taken from Chand & Gopal-Krishna (2012).

Gopal-Krishna, 2012). The estimated  $z_{in} \sim z_g$  are larger than BL Lacs but similar to quasars i.e.  $z_{in} < 1.25$  and these are summarised in Figure 13. FSRQs have to be observed through the ergosphere of a rotating black hole ie away from the poles, to explain the deduced distribution of  $z_g$  and which also explains the presence of wide emission lines in FSRQs.

These results then unequivocally support the suggestion in literature that blazars are quasars and possess the structure shown in Figure 12. BL Lacs are quasars viewed from the pole.

#### 3.1.2 Seyfert 1 galaxies

Spiral galaxies with a bright compact nucleus which showed emission lines similar to the lines detected in planetary nebulae were first identified by Seyfert (1943). These galaxies are now known as Seyfert galaxies. The nuclear emission lines were much broader ( $> 30 \text{ \AA}$ ) than those found in emission nebulae such as HII regions in our Galaxy or in neighbouring galaxies (Seyfert, 1943) thus indicating their distinct nature. It was also inferred that the maximum observed width of the hydrogen emission lines increased with absolute magnitude and with the ratio of light in the nucleus to the total light in the nebula (Seyfert, 1943). Since the central object in a Seyfert galaxy is also a black hole, we note that the large observed widths of the emission lines could be due to the varying gravitational potential across the emitting region as given by Eqn 10 while the increase in absolute magnitude could indicate proximity to the event horizon of the black hole. Absorption lines were also detected by Seyfert (1943) and were identified with the stellar spectrum from the galaxy. Seyfert galaxies were classified into two types based on their line spectra and referred to as type 1 and type 2 (Khachikian & Weedman, 1971). IUE detected absorption lines in the Seyfert 1 spectra which were blueshifted wrt emission features by upto  $2500 \text{ km s}^{-1}$  and these were inferred to have a non-stellar origin (Ulrich, 1988). Further observations with the Hubble Space Telescope (HST)

Table 4: Estimating the  $z_{\text{in}} \sim z_g$  component in the observed redshift of a sample of BL Lac objects for which Mg II absorption line redshifts have been recorded. Data is taken from Bergeron et al. (2011).

BL Lac objects	$z_{\text{em}}$	$z_{\text{MgII}} = z_c$	$z_g \sim z_{\text{in}}$
0100-337	0.875	0.6810	0.115
0238+1636	0.940	0.5245	0.272
0241+0043	0.989	0.6310	0.219
0334-4008	1.351	1.0791	0.130
0423-0120	0.915	0.6338	0.172
0428-3756	1.110	0.5592	0.353
0457-2324	1.003	0.8922	0.057
0538-4405	0.890	0.6725	0.130
0745-0044	0.994	0.7979	0.109
0909+0121	1.022	0.5369	0.316
0942-0047	1.362	0.8182	0.299
0948+0839	1.489	1.0763	0.199
1147-3812	1.049	0.3750	0.49
1408-0752	1.5	1.2753	0.099
1410+0203	1.253	1.1123	0.067
1427-4206	1.522	1.0432	0.234
1522-2730	1.294	1.2847	0.004
1743-0350	1.054	0.2527	0.639
1956-3225	1.242	0.6236	0.381
2031+1219	1.215	1.1158	0.047
2134-0153	1.285	1.2458	0.017
2225-0457	1.404	0.8458	0.302
0221+3556	0.944	0.6850	0.154

found that more than half the Seyfert 1 galaxies showed both emission and absorption lines in the nuclear spectrum and that high ionization lines like C IV were generally detected whereas few Seyfert 1 galaxies showed Mg II absorption lines (Crenshaw et al., 1999). The C IV doublet was detected in absorption at multiple blueshifted velocities wrt to the emission line and the absorption features of widths  $100\text{--}300 \text{ km s}^{-1}$  were resolved into several narrow kinematic components at high spectral resolution. Column densities of C IV ranging from  $10^{13\text{--}15} \text{ cm}^{-2}$  are estimated (Crenshaw et al., 1999). Crenshaw et al. (1999) also find an excellent correlation between the ultraviolet absorption features and X-ray 'warm absorbers' and infer that the two phenomena are related.

From the above discussion, it appears that quasars and Seyfert 1 galaxies share a few common properties: (1) compact bright nucleus (2) broad emission lines (3) multiple blue-shifted absorption lines. The main differences between the two types of objects are (1) quasars are observed at redshifts ranging from low to high ( $\sim 6$ ) whereas Seyferts are mostly observed at low redshifts. For example, all galaxies in a sample of 964 Seyfert galaxies (Lipovetsky et al., 1988) has a redshift  $z < 1$  with the median redshift being  $< 0.1$ , (2) the range of absorption line redshifts are accordingly lower in Seyfert 1 galaxies, (3) it is difficult to locate a host galaxy around a quasar whereas Seyfert nuclei are hosted in spiral galaxies.

Thus, we suggest that the basic structure of the nuclei of Seyfert 1 is same as a quasar in that there is a black

hole surrounded by degenerate matter surfaces and line forming matter. However the lower observed redshifts of Seyfert galaxies and hence the small contribution of gravitational redshifts to the observed line velocities indicates that the lines arise far from the event horizon. It is clear that matter is not located inside the ergosphere of a rotating black hole in Seyfert 1 nuclei. The multiple blue-shifted absorption lines detected in the spectra of Seyfert 1 nuclei indicate the varying separations of the absorbing zones from the black hole and hence the varying  $z_g$ . If we assume that a C IV 1548Å line of half width 30Å with  $z_g = 0.5$  (arises at  $R = R_s$ ) is observed from a quasar then Eqn. 10 tells us that the emitting region will be sheet-like i.e.  $\Delta R \sim 0.04R = 0.04R_s$ . However if the same line with the same parameters was observed from a low redshift Seyfert nucleus with  $z_g = 0.01$  (arises at  $R = 50R_s$ ) then Eqn. 10 estimates a thickness of  $\Delta R \sim 2R = 100R_s$  for the emitting layer around the black hole. Thus, observations and the inferred structure of quasars allows us to infer the following about Seyfert 1 galaxies : (1) the hot degenerate matter surface is located close to the event horizon giving the nucleus a compact bright morphology like quasars. (2) the nuclear line spectrum arises over a large region ( $100R_s$ ) from the event horizon as inferred from the low gravitational redshifts suffered by the lines and large line widths due to the varying gravitational potential. (3) the line forming shells are physically larger and tenuous than in quasars.

The above discussion can also be extended to other kind of active nuclei like those hosted in elliptical and Seyfert 2 galaxies and its properties similarly studied. From our study of quasars, blazars and Seyfert 1 galaxies above, we are convinced that the structure suggested for quasars in Figure 12 holds for all active nuclei with the differences in observed properties being due to (1) the separation between the degenerate matter surface and the event horizon and (2) the separation between the emitting and absorbing shells from the event horizon (3) rotation status of black holes.

The gravitational redshift shown by the spectral lines from all non-quasar active nuclei appear to be  $<< 0.5$ . However we caution against interpreting this result to mean that all non-quasar objects host a non-rotating black hole and all quasars host a rotating black hole. It might be likely that all active nuclei host a rotating black hole and the observational differences are only due to the varying location of the line forming regions. We should further understand observations before arriving at any conclusions regarding the spin of the black hole.

*In summary, we conclude that quasars are the most extreme form of an active nucleus with a structure shown in Figure 12. In case of other active nuclei the matter is located far from the event horizon and spread over large radial distances.*

## 4 Variability in quasars

Variability over several timescales ranging from minutes to years is observed in several active nuclei especially in quasars (includes blazars) and Seyfert 1 nuclei. The variability is generally confined to the continuum emission although there are reports of variability in the line strengths (e.g. Crenshaw et al., 1999). Here we restrict the discussion to variability in the continuum emission signal.

We recall that the continuum spectrum of quasars from optical to radio bands can be fitted by a power law likely to be synchrotron emission whereas thermal processes dominate the ultraviolet emission and also contribute to the optical emission. The location of the synchrotron emitting region wrt the black hole is not clear and hence we do not discuss variability in the synchrotron emission. However, since in the proposed structure, the black body continuum arises on the hot degenerate matter surface, it appears reasonable to suppose that any variability detected in the ultraviolet (and optical in many cases) will be due to an event on the degenerate matter surface. Thus, once the observed variability is established to be in the thermal emission, it can constrain the physical size of the emitting surface using light travel arguments and since this occurs close to the event horizon, the black hole mass can also be constrained. This can then complete the decoding of quasars. Using wavelengths other than ultraviolet and optical (in some cases) might require disentangling the power law and thermal contributions in its emission. For example, Matthews & Sandage (1963) found that while they could extrapolate the optical flux for 3C 48 and 3C 196 from the radio, it was not possible to do so for 3C 286 - one way to understand this would be that the optical emission in 3C 48 and 3C 196 is dominated by synchrotron emission whereas in 3C 286, it's a combination of synchrotron and thermal emission. 3C 48 showed variability  $\leq 15\text{m}$  (Matthews & Sandage, 1963). If we assume this arises on the degenerate matter surface (although it is likely to be synchrotron), then it indicates a physical size of  $2.7 \times 10^{13}$  cm and a black hole mass of  $10^8 M_{\odot}$ . However if the variability is in the synchrotron emission and arises far from the black hole, then this mass estimate will be wrong. For example, correlated variability is detected in radio, optical, ultraviolet, X-ray bands in the BL Lac object PKS 2155-304 with X-rays leading the other bands by 2-3 hours which indicates a synchrotron origin for the wideband variability (Edelson et al., 1995). Unless it is established that this synchrotron variability arises close to the black hole, it cannot be used to estimate the black hole mass.

A change of 45 % in the radio flux density was detected over a timescale of 3 hours in the blazar PKS 0537-441 (Romero et al., 1994). This indicates a physical size of  $\sim 3.2 \times 10^{14}$  cm. Rapid variability in the optical emission over a timescale of 1.5h was first detected in BL Lac objects (Miller et al., 1989). The light travel time argument constrains the size of the emitting region to  $\sim 1.5 \times 10^{14}$  cm. If the origin of this variability lies on the degenerate matter surface then it implies a black hole of mass  $\sim 10^9 M_{\odot}$  as suggested by Miller et al. (1989). Obviously some

Table 5: Estimating the  $z_{\text{in}} \sim z_g$  component in the observed redshift of a sample of  $\gamma$  ray bursts for which Mg II absorption line redshifts have been recorded. Data is taken from Prochter et al. (2006).

GRBs	$z_{\text{em}}$	$z_{\text{MgII}} = z_{\text{c}}$	$z_g \sim z_{\text{in}}$
GRB			
010222	1.477	0.927	0.285
020405	0.695	0.472	0.151
020813	1.255	1.224	0.014
021004	2.328	1.38	0.398
050505	4.275	1.695	0.957
050820	2.6147	0.692	1.136
050908	3.35	1.548	0.707
051111	1.55	1.190	0.164
060418	1.49	0.603	0.553
030323 <sup>1</sup>	3.37	1.4092	0.814

<sup>1</sup> From Vreeswijk et al. (2004)

assumption or a priori information regarding the location of the variability wrt to the black hole is needed to estimate the black hole mass, if at all. If it is localised to the degenerate matter surface then the timescales can be used to estimate the black hole mass.

In the next section we discuss one of the fastest and most energetic variable signal known i.e.  $\gamma$  ray bursts and show how these are related to quasars.

### 4.1 $\gamma$ Ray Burst (GRB)

GRBs were first reported by Klebesadel et al. (1973) as short bursts of duration  $\sim 0.1\text{s}$  to  $\sim 30\text{s}$  and time-integrated flux densities of  $10^{-5} - 2 \times 10^{-4}$  ergs  $\text{cm}^{-2}$  in the energy range of 0.2 to 1.5 MeV. Soon after the discovery of GRBs, the outbursts appeared to show two durations - short ( $< 1\text{s}$ ) and long ( $> 10\text{s}$ ). In the extensive data on the GRBs now available, a bimodal distribution in duration of the GRB with peaks centred around 0.5s and 50s has been noted. Such short timescale variability implies a compact emitting region of sizes  $\sim 1.5 \times 10^{10}$  cm and  $\sim 1.5 \times 10^{12}$  cm. If this region is close to the black hole then they imply masses of  $10^5$  and  $10^7 M_{\odot}$ . This, then suggests that low mass black holes can be responsible for GRBs. However we note that several longer duration GRBs and recurrent GRBs have also now been detected. This, then, can indicate a range of properties for the host object. We are also aware that two possible origins have been put forward to explain GRBs. An 'afterglow' emission was first detected in the X-ray (Costa et al., 1997) and has subsequently been detected in bands ranging from X-rays to radio.

Intriguingly, emission and absorption features have been detected in the afterglow spectrum of a GRB even at redshifts as high as  $\sim 6$  (e.g. Jensen et al., 2001) and which are similar to features in a quasar spectrum. Comparison of the incidence of absorption features due to Mg II in a GRB afterglow spectrum and quasars have found that former shows four times higher incidence of Mg II absorption as compared to quasars (Prochter et al., 2006) and

which has been difficult to understand in an intervening origin for the absorption features. On the other hand, the similarity of the absorption line spectra of quasars and GRBs have led to studies examining a possible connection between the two (Burbidge, 2003, 2007b). These studies have concluded that (1) one or more quasars are often found lying within a degree of a GRB, (2) the deduced redshifts of the absorption lines in a GRB spectrum show a periodicity similar to quasars (3) GRBs are local as also suggested for quasars and are ejected from a galaxy and (4) the observed redshifts are intrinsic. Keeping all this in mind, we use the same method as before to estimate the maximum  $z_g$  in a few GRBs. We use the data on 9 GRBs from Prochter et al. (2006) and the results are listed in Table 5. In this sample, the observed GRB redshifts range from 0.695 to 4.275;  $z_{MgII}$  ranges from 0.472 to 1.695 and  $z_{in} \sim z_g$  ranges from 0.014 to 1.136. *The remarkable result that  $z_{in} < 1.25$  is repeated for GRBs.* It appears too contrived to not conclude a definite connection between quasars and GRBs - and we suggest that GRBs are transient events on quasars. Recalling the unique structure of a quasar that observations argue for (see Figure 12) - the most probable origin of GRBs is in an event on the degenerate matter surface in quasars which subsequently leads to its brightening at multiple wavelengths in the afterglow. This is supported by the detection of emission and absorption lines in the afterglow. We argue that the afterglow is the brightening of the degenerate matter surface which then illuminates the surrounding emitting and absorbing shells and provides a glimpse into the structure of the parent quasar till the afterglow lasts. The quasar might be ‘dark’ and hence not detectable except after an explosive GRB event. The estimated values of  $z_g$  clearly indicate that matter is arranged inside the ergosphere of the rotating black hole in the host quasar. We note that apparent luminosities of GRBs can be as high as  $10^{54}$  erg  $s^{-1}$ . We search for possible causes of such an energetic transient event on a quasar.

We refer to the relatively well-understood Galactic phenomena of novae which brighten by 8 – 10 magnitudes in the optical in a very short time and which also emit  $\gamma$  rays. The most energetic novae are now well-established as being due to a cataclysmic thermonuclear explosion in accreted matter on the surface of a white dwarf. Since the proposed structure of a quasar has a degenerate matter surface surrounding the black hole, we reason that matter will be accreted onto it. This matter will get denser and hotter as it accumulates on the degenerate matter surface and can eventually ignite in a fast explosive thermonuclear burst which can release  $\gamma$  ray photons of energies of a few MeV. These low energy  $\gamma$  rays can be gravitationally boosted to higher energies due to the strong gravitational field of the black hole, before they leave the system. The explosion is soon quenched as observed from the short duration of the burst which gives an estimate of the size of the emitting region. We note that the luminosity of emission from the event horizon of a black hole can be boosted by a staggering factor of  $\sim 10^{27}$  and the black body temperature would appear to be boosted by a factor of  $\sim 4 \times 10^{13}$ !

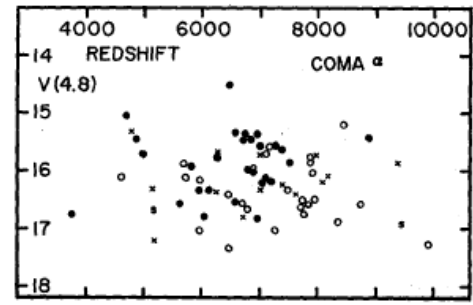


Figure 14: Redshift-magnitude correlation for member galaxies of Coma cluster. Filled circles are ellipticals, open circles are S0s, crosses are SB0 and s are spiral. Figure copied from Tift (1972).

(Shapiro & Teukolsky, 1983) which can easily explain the large luminosities of GRBs. The huge energy release will also brighten the degenerate matter surface in other wavebands and give rise to the multi-band afterglow of a GRB and the line spectrum. Once the afterglow becomes too faint, the spectrum also disappears. Piro et al. (1998) reported that the quasar 4C49.29 was located in a 3' radius circle around GRB 960720. We think many such correlations should exist otherwise it would mean that there exist ‘dark’ quasars which then contribute to dark matter and can only be detected gravitationally or through GRBs. Anyway, it is clear that a quasar should be present at the location of most GRBs unless there exist multiple origin paths to GRBs as has been suggested.

In summary, based on the observational results and the striking similarity of the spectra and estimated  $z_g$  with quasars, we suggest that GRBs are energetic thermonuclear explosions on the degenerate matter surface in a quasar similar to nova explosions on a white dwarf.

## 5 Other related topics

### 5.1 Nuclear redshift-magnitude bands in Coma cluster

In this section, we discuss how the explanation for the intriguing observational result of galaxies being arranged along bands in the nuclear redshift-magnitude diagram in the Coma cluster (Tift, 1972, 1973) as shown in Figure 14 emerges from what has been discussed so far in the paper. As Tift had pointed out, there are three contributions to the observed velocity of a Coma galaxy namely orbital motion in the cluster, Hubble expansion velocity of the cluster and an unknown origin. Tift (1972) concluded that the velocity dispersion in the Coma cluster is  $< 220$  kms $^{-1}$  thus attributing most of the observed velocity spread in the bands to an intrinsic origin.

We examine these results on Coma galaxies in light of our result that gravitational redshifts suffered by spectral lines arising in material close to the event horizon of a black hole can be as large as one. Thus the nuclear red-



shifts of galaxies which host a supermassive black hole in the centre can be assumed to include a non-zero contribution from  $z_g$ . While the nucleus will be brighter if the degenerate matter surface is closer to the black hole, it will also be obscured by the dense line forming material - the observed nuclear magnitude will vary from galaxy to galaxy depending on these two opposing effects. The bands in the magnitude-redshift diagram are best discernible when the nuclear magnitude is plotted against the nuclear redshift and are diluted once the signal from the entire galaxy is included. In light of all this, we can explain the result in Figure 14 as follows:

1. We suggest that the three bands are due to the orbital motion of the galaxies - the highest band indicates the receding galaxies and the lowest band indicates the approaching galaxies. The middle band indicates the galaxies which have no radial motion other than Hubble flow of the cluster towards us.
2. We suggest that the galaxies are located along a band depending on the contribution of the gravitational redshift to its nuclear spectrum and obscuration of its optical continuum from the degenerate matter surface by the line forming gas. Thus, the progressive shift of non-elliptical galaxies to fainter high redshift end would then indicate that both the gravitational redshift contribution and obscuration of degenerate matter surface is larger in non-ellipticals than in elliptical galaxies. This is as expected in the sense that non-ellipticals do have larger gas and dust fraction as compared to ellipticals. Moreover from the discussion till now, especially the presence of wide lines in quasars and Seyfert 1 spectra, it appears that the line forming gas in closest to the black hole in quasars followed by Seyfert 1 and then elliptical galaxies.

Interestingly, the above explanation and the arrangement of all galaxies along bands then indicates that all the galaxies in the Coma cluster host a central accreting black hole. Since the Coma cluster is virialised but not expected to be different, the result can be extrapolated to support the existence of a central supermassive black hole in all galaxies.

## 5.2 Formation of supermassive black holes - primordial?

Based on the observational results on quasars and active nuclei that are discussed in the paper and our inferences, it appears reasonable to support a primordial formation of supermassive black holes (Silk & Rees, 1998) around which matter arranged itself into galaxies. Thus the supermassive black holes could have formed first defining the location of galaxies. It would be interesting to examine the simple extrapolation that a disk galaxy formed around a rotating black hole whereas an elliptical galaxy formed around a non-rotating black hole. Quasars with their stellar-like compact appearance do not seem to be a

galaxy. Instead they appear to consist of the central supermassive black hole + dense gas shells surrounded by a spherical halo of gas in which low ionisation lines like Mg II form - more compact than normal galaxies. The existence of a supermassive black hole, dense matter shells, lack of an extended galaxy but hosting galaxy-like mass make one wonder if quasars are failed galaxies because all the matter rapidly fell in close to the central black hole during the phase of galaxy formation. With mounting evidence that all galaxies host a black hole at the centre including the explanation of Figure 14 presented in the previous section, the primordial origin appears to be gaining support. Interestingly, there seem to be studies which suggest that 20-30  $M_{\odot}$  black holes might also be primordial in nature (Kashlinsky, 2016). While stellar mass black holes can be understood as end products of massive stars, it has always been difficult to understand the origin of supermassive non-stellar mass black holes. Thus, the growing support for a primordial origin in which all galaxies should host a black hole at its centre appears to be a possible explanation. The kind of physical processes that can lead to such large masses being concentrated in such small regions needs to be explored.

## 6 Summary, conclusions, future

We have examined the origin of the continuum emission and the large redshifts shown by the emission and absorption lines in a quasar spectrum in the ultraviolet. The study has resulted in several important watertight inferences, all fitting together like a jigsaw puzzle and uniquely constraining the quasar structure. The important results/inferences can be summarised to be:

- All the emission and absorption lines detected in a quasar spectrum arise from matter inside the quasar system. The observed redshift ( $z = z_{em}$ ) of a quasar is large due to contribution from both the cosmological ( $z_c$ ) and intrinsic ( $z_{in}$ ) redshifts.  $z_{in}$  comprises of a Doppler component ( $z_D$ ) and a gravitational redshift ( $z_g$ ). We show that  $z_g$  going upto values of one comprises the dominant component of  $z_{in}$ .
- For quasars, we find  $z_c < z_{em}$ ,  $z_{in} < 1.25$  and  $z_c \leq 3$ .
- The observations, particularly in the ultraviolet band, determine a unique structure for a quasar. The proposed quasar structure consists of a supermassive black hole surrounded by degenerate matter shells (where the neutron and electron degeneracy pressure balance the black hole gravity) emitting thermal continuum peaking in the ultraviolet which heats and ionizes matter around it giving rise to a Stromgren shell where emission lines arise. Around the emitting shells are dense shells from where the absorption lines arise. The entire structure is arranged just outside the event horizon of a black hole in quasars (see Figure 12). The spectral lines are shifted by different  $z_g$  depending on the separation of the line forming region from the black hole i.e. gravitational potential.

This structure explains the enhanced ultraviolet continuum of quasars and the multiple redshifted spectral lines.

- We marvel at and believe that the existence of maximally gravitationally redshifted lines in quasar spectra are one of the most compelling proofs of Einstein's general theory of relativity (Einstein, 1915a,b,c,d). There is no doubt that there exist black holes with properties determined by the exact analytical solutions derived for non-rotating black holes by Schwarzschild (1916) and for rotating black holes by Kerr (1963). Quasars strongly support  $z_g$  upto 1 as expected for maximally rotating black holes and rule out  $z_g > 1$ .
- We suggest a method to separate  $z_c$  and  $z_{in}$  in a quasar spectrum. We assume that the lowest detected redshift of the Mg II absorption line  $z_{MgII}$  in a quasar spectrum includes no contribution from  $z_{in}$  and hence  $z_c = z_{MgII}$ . Using this, we find the remarkable result that the difference between the highest ( $z_{em}$ ) and lowest ( $z_{MgII}$ ) redshifts deduced in a quasar spectrum are  $< 1.25$ . This proves the existence of a non-trivial intrinsic redshift contribution to the velocity of the lines.
- Spectral lines from quasars show a  $z_g$  upto one.  $z_g \sim 0.5$  can be shown by lines arising in shells close to the Schwarzschild radius while  $z_g \sim 1$  is possible only from matter inside the ergosphere of a rotating black hole. This is the first time, to the best of our knowledge, that  $z_g$  between 0.5 and 1 has been inferred in astronomical spectral lines providing irrefutable evidence to the existence of rotating black holes and matter inside its ergosphere.
- The gravitational redshift component can trivially explain several intriguing observational results on quasars.
- We suggest that the peculiar morphology of the ergosphere is taken up by matter within as it arranges itself in equipotential shells around the black hole. The matter inside the ergosphere will resemble a thick accretion disk which is often postulated to exist around active nuclei.
- The emission and absorption lines detected in a quasar spectrum are broadened due to the varying gravitational potential in the line forming region and hence cannot be used to estimate the mass of the black hole.
- We find that  $z_g < 0.5$  for most BL Lac objects whereas  $z_g$  upto one is shown by spectral lines from FSRQs - both comprising blazars. Thus blazars are indeed quasars with the structure shown in Figure 12.
- We show that GRBs are transient events in quasars consisting of  $\gamma$  ray photons generated in an explosive thermonuclear reaction on the hot degenerate matter surface of the quasar. This explosion illuminates the degenerate matter surface giving rise to the multiband afterglow emission and a glimpse of the line spectrum of the quasar. It needs to be investigated whether this formation scenario explains all observed GRBs.
- We suggest the observed variability in quasars, especially in the ultraviolet continuum emission, can be unequivocally associated with energetic events on the degenerate matter surface - GRBs being the most energetic. Thus, the variability timescales alongwith the decoded shell structure from the observed gravitational redshifted lines should be able to uniquely constrain the quasar - black hole mass and the physical properties of the surrounding degenerate matter and line forming shells.
- The quasar model is applicable to other active nuclei with the variables being the separation between the black hole, degenerate matter surface and the line forming zones.
- We explain the band structure in the nuclear redshift-magnitude diagram shown by galaxies in the Coma cluster as being due to the effect of a gravitational redshift component and obscuration. This result strongly supports the presence of a supermassive black hole at the centres of all galaxies.
- Now that we have undeniable proof of the existence of matter inside the ergosphere of rotating black holes in quasars, it should be possible to further investigate how the energy of the black hole is tapped (e.g. Penrose, 1969; Blandford & Znajek, 1977).
- We now revisit the four questions posed in Section 2 and answer them based on the results: (1) the spectral lines arise inside the quasar; (2) quasars exist in the same volume as other active galaxies; (3) the ultraviolet continuum arises on the degenerate matter surface and a gravitational instability on the same leads to the some of the observed variability; (4) quasars are isolated black holes surrounded by matter with comparable masses but smaller physical sizes than galaxies.
- In light of the conclusive results on the presence of an intrinsic component in the quasar redshifts presented here, the suggestion that nearby galaxies and quasars/active nuclei are related (Arp, 1967, 1974) needs to be revisited.
- Now that we know that observed redshifts of quasars contain a sizeable redshift of non-cosmological origin, the existence and explanation of superluminal motions need to be revisited. For example, Cohen et al. (1971) inferred that while the quasars 3C273 and 3C279 showed superluminal expansion, the jets in the Seyfert galaxy NGC 1275 show non-superluminal expansion and in M87 show no expansion. This kind of gradation, if found to be widespread, could be due

to the wrong cosmological redshifts (and hence distance) which have been used for quasars (and to a lesser extent other active nuclei) and needs to be examined.

- The existence and implications of ‘dark’ quasars should be examined.
- Possibility of a gravitational redshift contribution to the Hubble constant should be examined.
- This research then gives us new questions to ponder on - for example: How are metals synthesized in quasars? What determines the separation between the event horizon and the line forming zones? Where does the synchrotron emission arise and is it due to a shock set up by the instability on the degenerate matter surface? What part of the structure of a quasar is common to the structure of any accreting black hole? Can we observe gravitationally redshifted lines from stellar mass black holes?

## Acknowledgements

I am grateful to all the researchers who have taken meticulous observations and drawn inferences from these data. Many research papers are cited here but many more have been referred to. I acknowledge generous use of ADS abstracts, arXiv, gnuplot, Wikipedia, LaTeX and Google search engines in this research.

## References

- Adams, W. S. 1925, Proceedings of the National Academy of Science, 11, 382
- Arp, H. 1966, ApJS, 14, 1
- . 1967, ApJ, 148, 321
- . 1971, Astrophys. Lett., 9, 1
- Arp, H. 1974, in IAU Symposium, Vol. 58, The Formation and Dynamics of Galaxies, ed. J. R. Shakeshaft, 199–218
- Bahcall, J. N., Peterson, B. A., & Schmidt, M. 1966, ApJ, 145, 369
- Bahcall, J. N. & Salpeter, E. E. 1966, ApJ, 144, 847
- Bahcall, J. N. & Spitzer, Jr., L. 1969, ApJ, 156, L63
- Bannister, N. P., Barstow, M. A., Holberg, J. B., & Bruhweiler, F. C. 2003, MNRAS, 341, 477
- Bergeron, J., Boissé, P., & Ménard, B. 2011, A&A, 525, A51
- Bergeron, J. & Kunth, D. 1983, MNRAS, 205, 1053
- Bergeron, J. & Stasińska, G. 1986, A&A, 169, 1
- Bertola, F., Burstein, D., Buson, L. M., Faber, S. M., & Lauer, T. R. 1987, in IAU Symposium, Vol. 127, Structure and Dynamics of Elliptical Galaxies, ed. P. T. de Zeeuw, 439
- Bica, E., Bonatto, C., Pastoriza, M. G., & Alloin, D. 1996, A&A, 313, 405
- Blandford, R. D. & Znajek, R. L. 1977, MNRAS, 179, 433
- Boksenberg, A. & Sargent, W. L. W. 2015, ApJS, 218, 7
- Burbidge, E. M. & Lynds, C. R. 1967, ApJ, 147, 388
- Burbidge, G. 2007a, ARA&A, 45, 1
- . 2007b, Philosophical Transactions of the Royal Society of London Series A, 365, 1357
- Burbidge, G., Burbidge, M., & Hoyle, F. 1967, ApJ, 147, 1219
- Burbidge, G. R. 2003, ApJ, 585, 112
- Burbidge, G. R. & Burbidge, E. M. 1967, ApJ, 148, L107
- . 1969, Nature, 222, 735
- Burbidge, G. R. & Hoyle, F. 1967, Nature, 216, 351
- Carswell, R. F., Coleman, G., Williams, R. E., & Strittmatter, P. A. 1976, A&A, 53, 275
- Chand, H. & Gopal-Krishna. 2012, ApJ, 754, 38
- Chen, S.-F. S., Simcoe, R. A., Torrey, P., Bañados, E., Cooksey, K., Cooper, T., Furesz, G., Matejek, M., Miller, D., Turner, M., Venemans, B., Decarli, R., Farina, E. P., Mazzucchelli, C., & Walter, F. 2016, ArXiv e-prints 1612.02829
- Cohen, M. H., Cannon, W., Purcell, G. H., Shaffer, D. B., Broderick, J. J., Kellermann, K. I., & Jauncey, D. L. 1971, ApJ, 170, 207
- Cooksey, K. L., Kao, M. M., Simcoe, R. A., O’Meara, J. M., & Prochaska, J. X. 2013, ApJ, 763, 37
- Costa, E., Frontera, F., Heise, J., Feroci, M., in’t Zand, J., Fiore, F., Cinti, M. N., Dal Fiume, D., Nicastro, L., Orlandini, M., Palazzi, E., Rapisarda, M., Zavatini, G., Jager, R., Parmar, A., Owens, A., Molendi, S., Cusumano, G., Maccarone, M. C., Giarrusso, S., Colletta, A., Antonelli, L. A., Giommi, P., Muller, J. M., Piro, L., & Butler, R. C. 1997, Nature, 387, 783
- Cottam, J., Paerels, F., & Mendez, M. 2002, Nature, 420, 51
- Crenshaw, D. M., Kraemer, S. B., Boggess, A., Maran, S. P., Mushotzky, R. F., & Wu, C.-C. 1999, ApJ, 516, 750
- Das, P. K. 1979, MNRAS, 186, 1
- Das, P. K. & Narlikar, J. V. 1975, MNRAS, 171, 87

- Dupree, A. K. & Raymond, J. C. 1983, *ApJ*, 275, L71
- Edelson, R., Krolik, J., Madejski, G., Maraschi, L., Pike, G., Urry, C. M., Brinkmann, W., Courvoisier, T. J.-L., Ellithorpe, J., Horne, K., Treves, A., Wagner, S., Wamsteker, W., Warwick, R., Aller, H. D., Aller, M. F., Ashley, M., Blecha, A., Bouchet, P., Bratschi, P., Bregman, J. N., Carini, M., Celotti, A., Donahue, M., Feigelson, E., Filippenko, A. V., Fink, H., George, I., Glass, I., Heidt, J., Hewitt, J., Hughes, P., Kollgaard, R., Kondo, Y., Koratkar, A., Leighly, K., Marscher, A., Martin, P. G., Matheson, T., Miller, H. R., Noble, J. C., O'Brien, P., Pian, E., Reichert, G., Saken, J. M., Shull, J. M., Sitko, M., Smith, P. S., Sun, W.-H., & Tagliaferri, G. 1995, *ApJ*, 438, 120
- Einstein, A. 1915a, *Sitzungsberichte der Königlich Preußischen Akademie der Wissenschaften (Berlin)*, Seite 844-847.
- . 1915b, *Sitzungsber. preuss.Akad. Wiss.*, vol. 47, No.2, pp. 831-839, 1915, 47, 831
- . 1915c, *Sitzungsberichte der Königlich Preußischen Akademie der Wissenschaften (Berlin)*, Seite 778-786.
- . 1915d, *Sitzungsberichte der Königlich Preußischen Akademie der Wissenschaften (Berlin)*, Seite 799-801.
- . 1920, *Relativity: The Special and General Theory* (English translation by Robert W. Lawson) (Methuen and Co Ltd)
- Fan, X., Strauss, M. A., Richards, G. T., Hennawi, J. F., Becker, R. H., White, R. L., Diamond-Stanic, A. M., Donley, J. L., Jiang, L., Kim, J. S., Vestergaard, M., Young, J. E., Gunn, J. E., Lupton, R. H., Knapp, G. R., Schneider, D. P., Brandt, W. N., Bahcall, N. A., Barentine, J. C., Brinkmann, J., Brewington, H. J., Fukugita, M., Harvanek, M., Kleinman, S. J., Krzesinski, J., Long, D., Neilsen, Jr., E. H., Nitta, A., Snedden, S. A., & Voges, W. 2006, *AJ*, 131, 1203
- Greenstein, J. L. & Matthews, M. S. 1957, *ApJ*, 126, 14
- Greenstein, J. L. & Schmidt, M. 1964, *ApJ*, 140, 1
- Greenstein, J. L. & Trimble, V. L. 1967, *ApJ*, 149, 283
- Gunn, J. E. & Peterson, B. A. 1965, *ApJ*, 142, 1633
- Holberg, J. B., Barstow, M. A., & Sion, E. M. 1998, *ApJS*, 119, 207
- Hoyle, F. & Burbidge, G. R. 1966, *ApJ*, 144, 534
- Hoyle, F. & Fowler, W. A. 1967, *Nature*, 213, 373
- Jensen, B. L., Fynbo, J. U., Gorosabel, J., Hjorth, J., Holland, S., Møller, P., Thomsen, B., Bjørnsson, G., Pedersen, H., Burud, I., Henden, A., Tanvir, N. R., Davis, C. J., Vreeswijk, P., Rol, E., Hurley, K., Cline, T., Trombka, J., McClanahan, T., Starr, R., Goldsten, J., Castro-Tirado, A. J., Greiner, J., Bailer-Jones, C. A. L., Kümmel, M., & Mundt, R. 2001, *A&A*, 370, 909
- Karlsson, K. G. 1971, *A&A*, 13, 333
- . 1990, *A&A*, 239, 50
- Kashlinsky, A. 2016, *ApJ*, 823, L25
- Kerr, R. P. 1963, *Physical Review Letters*, 11, 237
- Khachikian, E. Y. & Weedman, D. W. 1971, in *BAAS*, Vol. 3, *Bulletin of the American Astronomical Society*, 237
- Klebesadel, R. W., Strong, I. B., & Olson, R. A. 1973, *ApJ*, 182, L85
- Komossa, S., Xu, D., Zhou, H., Storchi-Bergmann, T., & Binette, L. 2008, *ApJ*, 680, 926
- Lipovetsky, V. A., Neizvestny, S. I., & Neizvestnaya, O. M. 1988, *Soobshcheniya Spetsial'noj Astrofizicheskoy Observatorii*, 55, 5
- Malkan, M. A. & Sargent, W. L. W. 1982, *ApJ*, 254, 22
- Matejek, M. S. & Simcoe, R. A. 2012, *ApJ*, 761, 112
- Mateo, M. & Szkody, P. 1984, *AJ*, 89, 863
- Matthews, T. A., Bolton, J. G., Greenstein, J. L., Munch, G., & Sandage, A. 1961, *S&T*, 21, 148
- Matthews, T. A. & Sandage, A. 1962, *PASP*, 74, 406
- Matthews, T. A. & Sandage, A. R. 1963, *ApJ*, 138, 30
- Miller, H. R., Carini, M. T., & Goodrich, B. D. 1989, *Nature*, 337, 627
- Panek, R. J. & Holm, A. V. 1984, *ApJ*, 277, 700
- Pavlov, G. G., Sanwal, D., Teter, M. A., & Zavlin, V. E. 2002, in *Bulletin of the American Astronomical Society*, Vol. 34, *American Astronomical Society Meeting Abstracts #200*, 780
- Penrose, R. 1969, *Nuovo Cimento Rivista Serie*, 1
- Piro, L., Heise, J., Jager, R., Costa, E., Frontera, F., Feroci, M., Muller, J. M., Amati, L., Cinti, M. N., dal Fiume, D., Nicastro, L., Orlandini, M., & Pizzichini, G. 1998, *A&A*, 329, 906
- Pound, R. V. & Rebka, G. A. 1960, *Physical Review Letters*, 4, 337
- Pound, R. V. & Snider, J. L. 1964, *Physical Review Letters*, 13, 539
- Prochter, G. E., Prochaska, J. X., Chen, H.-W., Bloom, J. S., Dessauges-Zavadsky, M., Foley, R. J., Lopez, S., Pettini, M., Dupree, A. K., & Guhathakurta, P. 2006, *ApJ*, 648, L93
- Raghunathan, S., Clowes, R. G., Campusano, L. E., Söchting, I. K., Graham, M. J., & Williger, G. M. 2016, *MNRAS*, 463, 2640

- Romero, G. E., Combi, J. A., & Colomb, F. R. 1994, *A&A*, 288
- Sargent, W. L. W., Boksenberg, A., & Steidel, C. C. 1988a, *ApJS*, 68, 539
- Sargent, W. L. W., Steidel, C. C., & Boksenberg, A. 1988b, *ApJ*, 334, 22
- Schmidt, M. 1963, *Nature*, 197, 1040
- . 1969, *ARA&A*, 7, 527
- Schneider, D. P., Schmidt, M., & Gunn, J. E. 1991, *AJ*, 102, 837
- Schwarzschild, K. 1916, *Sitzungsberichte der Königlich Preußischen Akademie der Wissenschaften (Berlin)*, 1916, Seite 189-196
- Seyfert, C. K. 1943, *ApJ*, 97, 28
- Seyffert, E. N., Cooksey, K. L., Simcoe, R. A., O'Meara, J. M., Kao, M. M., & Prochaska, J. X. 2013, *ApJ*, 779, 161
- Shapiro, S. L. & Teukolsky, S. A. 1983, *Black holes, white dwarfs, and neutron stars: The physics of compact objects*
- Shen, Y., Brandt, W. N., Denney, K. D., Greene, J. E., Grier, C. J., Ho, L. C., Peterson, B. M., Petitjean, P., Richards, G. T., Schneider, D. P., Tao, C., & Trump, J. R. 2016, *ArXiv e-prints*
- Silk, J. & Rees, M. J. 1998, *A&A*, 331, L1
- Strittmatter, P. A., Carswell, R. F., Burbidge, E. M., Hazard, C., Baldwin, J. A., Robinson, L., & Wampler, E. J. 1973, *ApJ*, 183, 767
- Strittmatter, P. A. & Williams, R. E. 1976, *ARA&A*, 14, 307
- Sun, W.-H. & Malkan, M. A. 1989, *ApJ*, 346, 68
- Terrell, J. 1964, *Science*, 145, 918
- . 1966, *Science*, 154, 1281
- Tifft, W. G. 1972, *ApJ*, 175, 613
- . 1973, *ApJ*, 179, 29
- . 1980, *ApJ*, 236, 70
- Tytler, D. & Fan, X.-M. 1992, *ApJS*, 79, 1
- Ulrich, M.-H. 1988, *MNRAS*, 230, 121
- Vanden Berk, D. E., Richards, G. T., Bauer, A., Strauss, M. A., Schneider, D. P., Heckman, T. M., York, D. G., Hall, P. B., Fan, X., Knapp, G. R., Anderson, S. F., Annis, J., Bahcall, N. A., Bernardi, M., Briggs, J. W., Brinkmann, J., Brunner, R., Burles, S., Carey, L., Castander, F. J., Connolly, A. J., Crocker, J. H., Csabai, I., Doi, M., Finkbeiner, D., Friedman, S., Frieman, J. A., Fukugita, M., Gunn, J. E., Hennessey, G. S., Ivezić, Ž., Kent, S., Kunszt, P. Z., Lamb, D. Q., Leger, R. F., Long, D. C., Loveday, J., Lupton, R. H., Meiksin, A., Merelli, A., Munn, J. A., Newberg, H. J., Newcomb, M., Nichol, R. C., Owen, R., Pier, J. R., Pope, A., Rockosi, C. M., Schlegel, D. J., Siegmund, W. A., Smee, S., Snir, Y., Stoughton, C., Stubbs, C., SubbaRao, M., Szalay, A. S., Szokoly, G. P., Tremonti, C., Uomoto, A., Waddell, P., Yanny, B., & Zheng, W. 2001, *AJ*, 122, 549
- Vreeswijk, P. M., Ellison, S. L., Ledoux, C., Wijers, R. A. M. J., Fynbo, J. P. U., Møller, P., Henden, A., Hjorth, J., Masi, G., Rol, E., Jensen, B. L., Tanvir, N., Levan, A., Castro Cerón, J. M., Gorosabel, J., Castro-Tirado, A. J., Fruchter, A. S., Kouveliotou, C., Burud, I., Rhoads, J., Masetti, N., Palazzi, E., Pian, E., Pedersen, H., Kaper, L., Gilmore, A., Kilmartin, P., Buckle, J. V., Seigar, M. S., Hartmann, D. H., Lindsay, K., & van den Heuvel, E. P. J. 2004, *A&A*, 419, 927
- Weymann, R. J., Carswell, R. F., & Smith, M. G. 1981, *ARA&A*, 19, 41
- Zapolsky, H. S. 1968, *ApJ*, 153, L163



# ERRATA & COMMENTS on Decoding quasars: gravitationally redshifted spectral lines!

Nimisha G. Kantharia

National Centre for Radio Astrophysics,  
Tata Institute of Fundamental Research,  
Post Bag 3, Ganeshkhind, Pune-411007

Email: [nkprasadnetra@gmail.com](mailto:nkprasadnetra@gmail.com)

URL: <https://sites.google.com/view/ngkresearch/home>

**December 2017**

This appended document lists and corrects errors in the paper and includes comments relevant to the paper. The numbering of figures, tables and equations is independent of the paper. The few references which are referred to in this document are included in the reference list of the paper. Further errors if and when identified will be updated at <https://sites.google.com/view/ngkresearch/home>.

1. The wavelength part of Equations 4, 6 in the paper are wrong and these are corrected here. The frequency formula is correct. The correct form for Equation 4 is the following:

$$\frac{\nu_0 - \nu}{\nu_0} = \frac{GM}{Rc^2} \quad \text{or} \quad \frac{\lambda - \lambda_0}{\lambda} = \frac{GM}{Rc^2}$$

and the correct form for Equation 6 is:

$$z_g(R) = \frac{\lambda_{\text{obs}} - \lambda_{\text{rest}}}{\lambda_{\text{obs}}} = \frac{GM}{Rc^2} = \frac{v}{c}$$

This, leads to the recognition of a major update that is required in the paper which is elaborated in point 5 in this document. (*September 2017*)

2. Figure 6 in the paper gives a schematic structure of the event horizon, ergosphere and ergosurface around a rotating black hole as is conventionally shown in literature. However it fails to represent the following important points for a rotating black hole: (1) The event horizon of a maximally rotating black hole is prolate-shaped with its semi-major axis which is along the polar axis being equal to the Schwarzschild radius  $R_s$  and its semi-minor axis which is in the equatorial plane being equal to half the Schwarzschild radius. For black holes with lower rotation speeds, the semi-minor axis of the event horizon will lie between  $R_s$  and  $R_s/2$ . (2) The ergosphere of a rotating black hole is the region between the prolate-shaped event horizon and the pseudo-surface of a sphere of radius  $R_s$  known as the ergosurface. The corrected schematic is shown in Figure 1. We also include an extra schematic for a non-rotating black hole in the figure. (*September 2017*)
3. Figure 12 in the paper showing the proposed structure of a quasar is modified to include the correct structure of a rotating black hole as depicted in Figure 6. The corrected figure is shown in Figure 2. There is no change in the detailed structure of a quasar i.e the degenerate surfaces and line forming regions (when a gravitational redshift  $> 0.5$  is inferred) continue to be located inside the ergosphere and are shown. The line-forming matter located beyond  $R_s$  from the black hole will show a gravitational redshift  $> 0.5$ . (*September 2017*)
4. Alongwith the updated schematics, we include a few points here which we can surmise from observations and black hole physics since there seems to prevail some confusion in literature:
  - The event horizon is the fictitious surface around the black hole which defines a surface of no-return for both light and matter. As shown in the paper, the quasar spectrum arises from matter located just outside this surface. Observations support the prolate-shaped structure for the event horizon in rotating black holes so that its radius varies from  $R_s/2$  to  $R_s$  at the equator (depending on its rotation speed) but is always  $R_s$  at the poles.
  - The event horizon is a pseudo-surface of a sphere of radius  $R_s$  around a non-rotating black hole while it is a prolate-shaped pseudo-surface which is located inside the sphere of radius  $R_s$  in a rotating black hole. In a rotating black hole, the pseudo-surface of radius  $R_s$  around the black hole is referred to as the ergosurface. The region between the event horizon and the ergosurface in a rotating black hole is the ergosphere. In a non-rotating black hole, the event horizon and ergosurface are the same and there is no ergosphere. The escape velocity from the event horizon in a non-rotating black hole and ergosurface in a rotating black hole is equal to velocity of light. The escape velocity from inside the ergosphere has to be  $\geq$  velocity of light. As quasar spectra demonstrate, electromagnetic radiation can escape from within the ergosphere and indicates that the escape velocity continues to be equal to velocity of light inside the ergosphere also. We have no

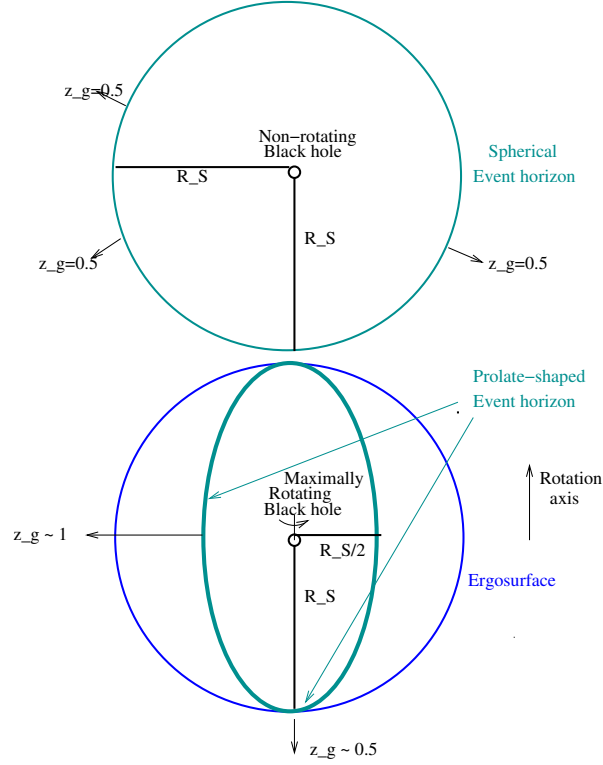


Figure 1: **Figure 6 in the paper should be replaced by this figure.**  $R_s$  denotes Schwarzschild radius,  $z_g$  denotes gravitational redshift. The edits in the schematic is in the shape of the event horizon and ergosphere and inclusion of a schematic for a non-rotating black hole. Rotation of the black hole leads to the event horizon moving inwards in the non-polar regions and the appearance of a region known as the ergosphere which becomes visible. For a non-rotating black hole, the maximum  $z_g < 0.5$  while for a rotating black hole, the maximum  $z_g < 1$ .

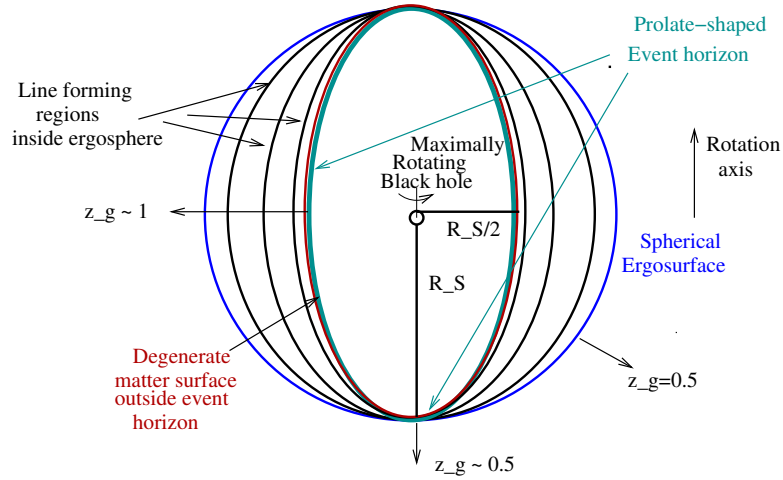


Figure 2: **Figure 12 in the paper should be replaced by this figure.**  $R_s$  denotes Schwarzschild radius,  $z_g$  denotes gravitational redshift. The edit is in the shape of the event horizon (prolate-shaped ellipse) and ergosphere (spherical) of the maximally rotating black hole. The maximum gravitational redshift that lines forming just outside the event horizon at the equator can suffer is  $< 1$  whereas those forming outside the event horizon at the poles can suffer  $z_g < 0.5$  in a rotating black hole. The lines forming in matter outside the pseudo-surface of radius  $R_s$  in both types of black holes will show a shift  $z_g < 0.5$ .

evidence of matter escaping from the ergosphere and no matter should be able to escape from the ergosphere since the escape velocity from the ergosphere is equal to the velocity of light. So matter once trapped inside the ergosphere can never escape but can only fall into the black hole. This can also be understood as follows:  $1/2 mv_{esc}^2 = GmM/R^2$  so that  $v_{esc} = \sqrt{(2GM/R)}$ . Schwarzschild radius is  $R_s = 2GM/c^2$  so that at this distance (event horizon or ergosurface),  $v_{esc} = c$  (Schwarzschild radius is defined by this criterion). We note that  $z_g = GM/Rc^2 = R_s/2R$  so that the multi-redshifted spectral lines in a quasar spectrum which show a gravitational redshift  $z_g \leq 0.5$  will arise from the pseudo-surface of radius  $R_s$  or beyond it while if  $z_g > 0.5$ , then the lines have to arise from matter located within  $R_s$  i.e. within the ergosphere. Since we are able to observe these spectral lines means that light is able to escape from the ergosphere and indicates that the escape velocity continues to be  $c$  within the ergosphere.

- One often encounters mention of an inner and outer event horizon in literature. It appears that these refer to the event horizon and the ergosurface in a rotating black hole. The terminology might have come into practise since both will be pseudo-surfaces of equal effective potential and different gravitational potential. One can think of the ergosphere as a ‘stretching’ of the event horizon in rotating black holes which allows us an electromagnetic glimpse into a region around the black hole which would not have been possible in a non-rotating black hole. Thus, while observations unequivocally prove the existence of rotating black holes (from spectral lines which show  $z_g \geq 0.5$ ), it appears more difficult to prove the existence of non-rotating black holes or rather disentangling the observational signatures of non-rotating black holes from rotating black holes since the lines with  $z_g < 0.5$  can arise from matter around both types of black holes. Since most astrophysical systems show rotation, it might be that all black holes are also rotating. However it needs to be investigated using observational results.

(September 2017)

5. Reflecting more on the implications of the different wavelength-redshift conversion formula for estimating cosmological and gravitational redshifts, it is found that a major update to the paper is required. This edit does not change the interpretation in that the results continue to support the intrinsic origin of the entire quasar spectrum as shown in the paper and in fact strengthens the inferences, nevertheless this update is very critical and crucial to the correctness of the paper. While it is still advocated that the intrinsic redshift is a measure of the gravitational redshift, it is realised that they cannot be equal. A conversion factor needs to be applied to the intrinsic redshift to convert it into gravitational redshift. This conversion has not been included in the paper and is the fault that this update aims to correct.

The quasar redshift ( $z$  or  $z_{em}$ ) is estimated from the observed and rest wavelengths of the emission line in the quasar spectrum as follows:

$$z = \frac{\lambda_{\text{obs}} - \lambda_{\text{rest}}}{\lambda_{\text{rest}}} \quad (1)$$

Equation 1 of the paper which was  $((1+z) = (1+z_c)(1+z_{in}))$  indicates that in the general case, the observed redshift of the emission line  $z$  will be a combination of an intrinsic redshift  $z_{in}$  and an extrinsic i.e. cosmological redshift  $z_c$ . The same will be true for the absorption lines which are observed in the quasar spectrum. While the cosmological redshift will be the same for all the spectral lines which arise within the quasar, it will differ if the spectral lines arise at different locations along the sightline to the quasar. The spectral lines which arise within the quasar can suffer different intrinsic redshifts due to some physical process in the quasar but will all have the same cosmological redshift. In the paper, this second scenario in which the observed redshifts contained a constant contribution from cosmological redshift and a varying component due to an intrinsic process was examined in detail. A method for separating the two components was suggested and it was shown that multiple redshifts of lines in the spectrum to a quasar were expected due to the effect of a varying gravitational potential if the lines arose close to but at different radial separations from the event horizon of the supermassive black hole in the quasar. Thus, photons arising in the radially varying strong gravitational potential of the black hole and hence gravitational redshifted was shown to be the intrinsic process which could explain the observed multi-redshifted quasar spectrum and was a very plausible alternative to the intervening matter scenario. However as mentioned above, a mistake was made in the paper in assuming that the gravitational redshift was the same as the intrinsic redshift estimated from  $z$  and  $z_c$ . We explain this below and provide the corrected form for estimating gravitational redshifts. The gravitational redshifts thus found for the emission/absorption lines of quasars listed in tables in the paper are included here. Two figures are also accordingly updated. The y-axis label of Figure 8 in the paper should be changed to ‘Intrinsic redshift  $z_{in}$ ’.

While both  $z_c$  and  $z_{in}$  are related to the shifted wavelength due to the respective process i.e.  $\lambda_{obs,c}$  and  $\lambda_{obs,in}$  as

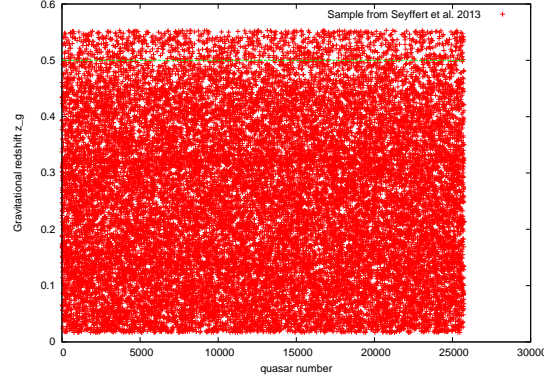
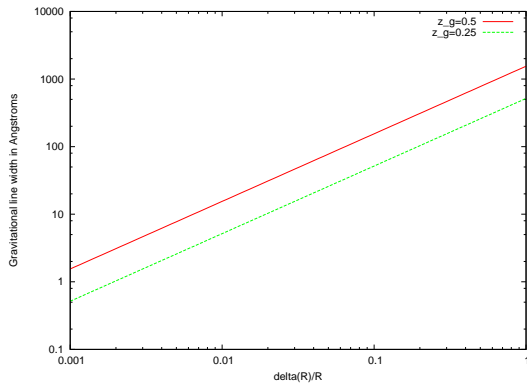


Figure 3: The largest gravitational redshift detected in a quasar spectrum estimated using the above procedure for the sample of absorption line quasars from the Seyffert et al. (2013) sample. The horizontal line is drawn at  $z_g = 0.5$ . The emission lines which show  $z_g$  above this line form in matter inside the ergosphere. The median  $z_g = 0.25$ .

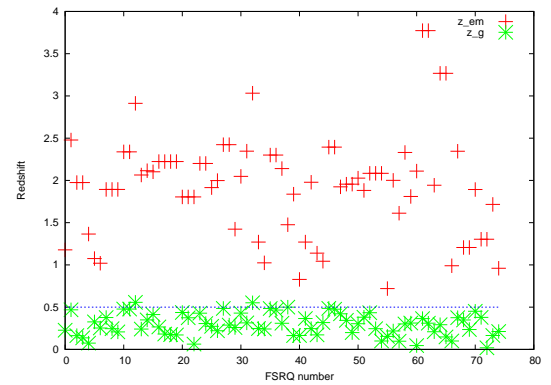
given in Equation 1, the gravitational redshift  $z_g$  of a spectral line can be estimated from the wavelengths as:

$$z_g = \frac{\lambda_{\text{obs},g} - \lambda_{\text{rest}}}{\lambda_{\text{obs},g}} \quad (2)$$

where the subscript  $g$  refers to the wavelength shift arising due to gravitational redshift. The intrinsic redshift of the spectral lines in a quasar spectrum are shown to be caused by the physical process which is responsible for gravitational redshifts and hence  $\lambda_{\text{obs},g} = \lambda_{\text{obs},in}$  (other possible intrinsic processes such as Doppler expansion are ignored) i.e. the wavelength shift of a line due to intrinsic redshift and gravitational redshift is the same. However since the denominators in Equations 1 and 2 are different;  $z_{in} \neq z_g$ . **So the major change required in the paper is to replace the heading of  $z_g$  in the tables and plotted quantity of  $z_g$  in figures by  $z_{in}$ .  $z_{in}$  is a measure of  $z_g$  but  $z_{in} \neq z_g$ . An extra factor is required for converting  $z_{in}$  to  $z_g$ .**



(a)



(b)

Figure 4: (a) Modified Figure 9 in the paper after using the correct equation for  $z_g$  to estimate the observed wavelength of the redshifted line of C IV 1548 Å. The plots are shown for  $z_g = 0.5$  and  $z_g = 0.25$ . (b) An additional panel for Figure 13, is presented here. In the paper, Figure 13 plotted the intrinsic redshift distribution for a sample of flat spectrum radio quasars whereas here the gravitational redshift distribution the same sample is shown. The horizontal line is drawn at 0.5.

To recall, we have determined the  $z_{in}$  of the emission line from the difference between the quasar redshift (emission line redshift i.e. highest redshift in the quasar spectrum,  $z$ ) and the lowest redshift at which Mg II absorption doublet lines are detected (i.e. lowest redshift in the quasar spectrum,  $z_c$ ) by assuming that the lowest redshift in the quasar spectrum is the true indicator of the distance to the quasar i.e. is the cosmological redshift. The estimated  $z_{in}$  is related to the observed and rest wavelength as in Equation 1 and hence we can express  $\lambda_{\text{obs},in}$  in

Table 1: Tables 1,3,4,5 in the paper list what was thought to be  $z_g$  but as pointed out here, the listed values are of  $z_{in}$ . So the heading in the tables in the paper should be exclusively ' $z_{in}$ '. The gravitational redshifts  $z_g$  estimated from  $z_{in}$  using Equation 4 are listed here for the same objects listed in the tables.  $z_{in}$  which is already tabulated in the tables in the paper is also included.

Table 1			Table 3			Table 4			Table 5		
Quasar	$z_{in}$	$z_g$	Quasar	$z_{in}$	$z_g$	BL Lac	$z_{in}$	$z_g$	GRB	$z_{in}$	$z_g$
Q0013-004	1.133	0.531	Q048+163(em)	0.844	0.457	0100-337	0.115	0.103	010222	0.285	0.221
Q0014+818	1.073	0.517	Q048+163	0.5493	0.354	0238+1636	0.272	0.213	020405	0.151	0.131
Q0058+019	0.835	0.455	Q048+163	0.5562	0.357	0241+0043	0.219	0.179	020813	0.014	0.0138
Q0119-046	0.772	0.435	Q048+163	0.5574	0.357	0334-4008	0.130	0.115	021004	0.398	0.284
Q0150-203	1.265	0.558	Q048+163	0.8383	0.456	0423-0120	0.172	0.146	050505	0.957	0.489
Q0207-003	0.883	0.468	Q0014+818(em)	1.073	0.517	0428-3756	0.353	0.260	050820	1.136	0.531
Q0229+131	1.235	0.552	Q0014+818	0.6548	0.395	0457-2324	0.057	0.0539	050908	0.707	0.414
Q0348+061	1.186	0.542	Q0014+818	0.7992	0.444	0538-4405	0.130	0.115	051111	0.164	0.140
Q0440-168	0.833	0.454	Q0014+818	0.8004	0.444	0745-0044	0.109	0.0982	060418	0.553	0.356
Q0450-132	1.177	0.540	Q0014+818	1.0022	0.500	0909+0121	0.316	0.240	030323	0.814	0.448
Q0528-250	0.937	0.483	Q0837+109(em)	0.7561	0.430	0942-0047	0.299	0.230			
Q0837+109	0.756	0.430	Q0837+109	0.3869	0.278	0948+0839	0.199	0.165			
Q0848+163	0.844	0.457	Q0837+109	0.6058	0.377	1147-3812	0.49	0.328			
Q0852+197	1.276	0.560	Q0837+109	0.6817	0.405	1408-0752	0.099	0.0900			
Q0958+551	1.216	0.548	54452-2824-554(em)	0.1531	0.132	1410+0203	0.067	0.0627			
Q1222+228	0.822	0.451	54452-2824-554	0.0011	0.001	1427-4206	0.234	0.189			
Q1329+412	0.955	0.488	54452-2824-554	0.02	0.0196	1522-2730	0.004	0.0039			
Q1331+170	0.768	0.434	54452-2824-554	0.0419	0.040	1743-0350	0.639	0.389			
Q1517+239	0.667	0.400	54452-2824-554	0.0965	0.0883	1956-3225	0.381	0.275			
Q1548+093	1.118	0.527	52178-0702-503(em)	1.0163	0.504	2031+1219	0.047	0.0442			
Q1623+269	0.868	0.464	52178-0702-503	0.7305	0.422	2134-0153	0.017	0.016			
Q1715+535	1.142	0.533	52178-0702-503	0.7386	0.424	2225-0457	0.302	0.231			
Q2206-199	1.031	0.507	52178-0702-503	0.7629	0.432	0221+3556	0.154	0.133			
Q2342+089	1.196	0.544	52178-0702-503	0.9220	0.479						
Q2343+125	1.03	0.507	52618-1059-146(em)	0.6783	0.404						
Q2344+125	0.839	0.456	52618-1059-146	0.4402	0.305						
Q2145+067	0.112	0.100	52618-1059-146	0.4769	0.322						
			52618-1059-146	0.5432	0.351						

terms of  $\lambda_{rest}$  as follows:

$$\lambda_{obs,in} = (z_{in} + 1)\lambda_{rest} \quad (3)$$

Since  $\lambda_{obs,in} = \lambda_{obs,g}$ , we can substitute for  $\lambda_{obs,g}$  in Equation 2 from Equation 3, so that  $z_g$  is expressed in terms of  $z_{in}$  which we have already estimated:

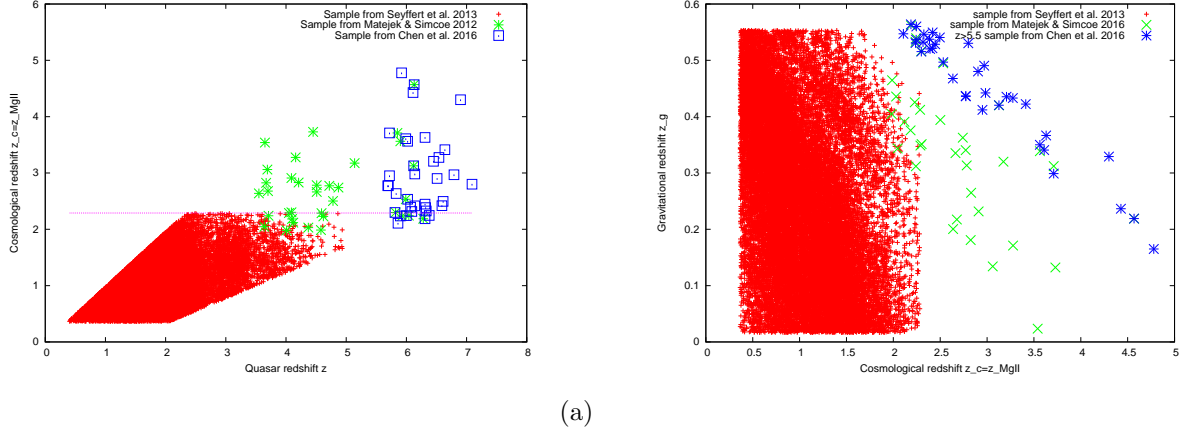
$$z_g = \frac{(z_{in} + 1)\lambda_{rest} - \lambda_{rest}}{(z_{in} + 1)\lambda_{rest}} = \frac{z_{in}}{(z_{in} + 1)} \quad (4)$$

**The gravitational redshift  $z_g$  can be determined by dividing  $z_{in}$  by the factor  $z_{in} + 1$ .**

The gravitational redshifts contributing to the quasar redshift has been estimated as above for the sample of quasars from Seyffert et al. (2013) that has been used in the paper and the resulting distribution of gravitational redshifts of the emission lines is shown in Figure 3. The median value of  $z_g$  is 0.25. In Table 1, we include the emission line gravitational redshifts for the quasars listed in Tables 1,3,4,5 in the paper. This change should also lead to edits in the text of the paper but for now it is considered crucial to point out this update and update the tables especially since the main inferences of the paper remain unchanged.

Another edit is related to Equation 10 in the paper which implicitly uses  $z_g$ . Figure 9 in the paper plots the gravitational linewidth for different  $z_g$  and the expected fractional thickness of the line forming zone. The corrected figure is shown in Figure 4(a) for gravitational redshifts of 0.5 and 0.25 and should replace Figure 9 in the paper. Since the shifted wavelength of a line, given a gravitational redshift can be estimated as  $\lambda_{obs,g} = \frac{\lambda_{rest}}{(1-z_g)}$ , the displaced wavelength of the 1548 Å line will be 3096 Å for  $z_g = 0.5$  and will be 2064 Å for  $z_g = 0.25$ .

Figure 13 in the paper shows the distribution of the redshift of the flat spectrum radio quasars (FSRQ) and the estimated intrinsic redshift. We show the distribution of gravitational redshifts estimated from  $z_{in}$  as detailed above in Figure 4(b) here. (November 2017)



(a)

Figure 5: (a) The lowest redshift of the Mg II absorption feature in the quasar spectrum taken from Seyffert et al. (2013) (red cross), Matejek & Simcoe (2012) (green star) and for the  $z > 5.5$  sample of quasars from Chen et al. (2016) (blue box). The horizontal line is drawn at a redshift of 2.29. (b) Figure shows the distribution of  $z_g$  estimated using Equation 2 against  $z_c = z_{\text{MgII}}$  for the sample of quasars in Seyffert et al. (2013); Matejek & Simcoe (2012); Chen et al. (2016). Note that the quasars with redshift  $< 1.5$  from the sample in Seyffert et al. (2013) show the entire range of  $z_g$  (from 0.0166 to 0.5535) and the largest gravitational redshift observed appears to decrease as  $z_c$  increases for  $z_c > 1.5$ . However quasars with high  $z_c$  from Chen et al. (2016) does show large values of  $z_g$  indicating decreasing  $z_g$  with  $z_c$  might also a result of observational bias since the number of high redshift quasars and high  $z_{\text{MgII}}$  searches are limited.

6. Alongwith the update in point 5, we also show a few results derived from datasets listing Mg II absorption redshifts detected towards quasars and which also include higher redshift quasars than were discussed in the paper. We find that this analysis also supports a non-trivial contribution to the observed redshift of spectral lines in quasar spectra by an intrinsic process in the quasar. The sample of the Mg II absorption line redshifts in the range 0.35 to 2.3 in Seyffert et al. (2013); Raghunathan et al. (2016) and the samples of quasars which list Mg II absorption in the redshift range of 2 to 7 from Matejek & Simcoe (2012); Chen et al. (2016) were analysed. The results are shown in Figures 5,6 and the estimated  $z_g$  for the high redshift quasars ( $z > 3.5$ ) from Matejek & Simcoe (2012); Chen et al. (2016) are listed in Table 2. The gravitational redshift ( $z_g$ ) component in the emission line redshift ( $z = z_{\text{em}}$ ) is estimated using the procedure suggested in the paper and also includes the last step specified in Equation 4 in point 5. The important inputs to the procedure are emission line redshift of the quasar  $z$  and  $z_c$  which is the lowest redshift at which Mg II absorption is detected in a quasar spectrum - the difference redshift is  $z_{\text{in}}$  which is a measure of  $z_g$ . Since the emission line shows the largest redshift in a quasar spectrum, this method estimates the largest  $z_g$  in the spectrum. If the absorption line redshifts are used instead of  $z_{\text{em}}$ , then the gravitational redshift component in those redshifts can be estimated in the same way.

Examining the distribution of the lowest redshift of the Mg II absorption (range 0.3 to 2.5) detected along a quasar sightline shown in Figure 5a, we note that the sample of quasars from Seyffert et al. (2013) show a trapezium-shaped distribution in the  $z \rightarrow z_{\text{MgII}}$  plane. The higher redshift sample from Matejek & Simcoe (2012); Chen et al. (2016) are also distributed in a similar fashion. We focus on the observed distribution of  $z_{\text{MgII}}$  in the larger sample from Seyffert et al. (2013). The upper ( $z_{\text{MgII}} \sim 2.3$ ) and lower ( $z_{\text{MgII}} \sim 0.35$ ) bounds are due to the redshift limits of the Mg II catalogue. The left slanting side indicates the largest value of  $z_{\text{MgII}} = z_c$  i.e. the maximum  $z_c$  detected in the sample for a given quasar redshift. The right slanting side of the trapezium indicates the minimum  $z_{\text{MgII}} = z_c$  that is detected in the sample for a given quasar redshift. The largest and smallest  $z_{\text{MgII}} = z_c$  at any given  $z$  is the range of  $z_{\text{MgII}} = z_c$  observed for that quasar redshift within the catalogue bounds. While upto  $z \sim 2$ , the smallest  $z_{\text{MgII}}$  detected in the sample continues to be  $\sim 0.35$  which is the lower limit of the range of explored redshifts in the catalogue, for  $z \geq 2.2$ , there are no quasars for which  $z_{\text{MgII}}$  is  $\sim 0.35$ . The smallest redshift at which Mg II absorption is detected for a given quasar redshift keeps increasing with  $z$  beyond  $z \sim 2.2$ . For example, none of the quasars with  $z > 3$  have recorded Mg II absorption with  $z_{\text{MgII}} < 0.7$ . We examine the behaviour of the detected Mg II redshifts, in the context of the two types of origin of these features namely external, in the intervening clouds along the sightline and intrinsic to the quasar. In the intervening cloud origin, we would have expected the smallest  $z_{\text{MgII}}$  detected at all quasar redshifts to be constant and in this case equal to the lower bound of the range of explored redshifts i.e. 0.35, since at least a few high redshift quasars should have sightlines passing through the nearby Mg II clouds. Since there is not a single detection of the nearby clouds in the high redshift quasars (see Figure 5a) i.e. low  $z_{\text{MgII}}$  features are missing in



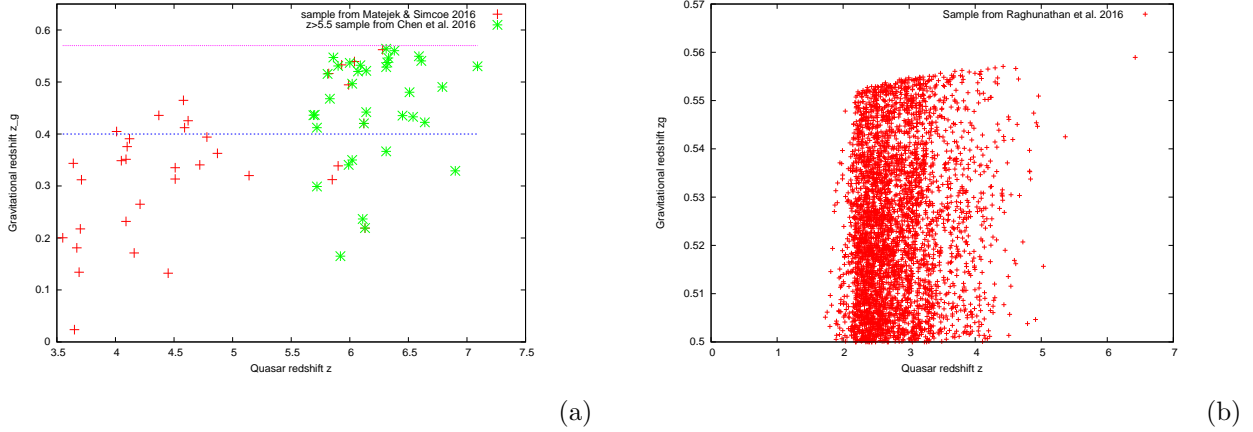


Figure 6: (a) Distribution of gravitational redshifts estimated for the sample with  $z > 3.5$  in Matejek & Simcoe (2012) and  $z > 5.5$  in Chen et al. (2016). Horizontal lines are drawn at 0.4 and 0.57. Notice the predominance of larger gravitational redshift for the larger quasar redshifts i.e. the fraction of quasars with  $z > 5.5$  having maximum  $z_g$  between 0.4 and 0.57 is larger than compared to quasars with  $z < 5.5$ . This is expected if the increasing quasar redshift is due to increasing contribution from both  $z_c$  and  $z_g$ . (b) A zoom-in into the  $z_g$  range of 0.5 to 0.57 for the sample of quasars in Raghunathan et al. (2016) shows the same trend as in (a) i.e. an increasing largest  $z_g$  with  $z$  in the quasar redshift range of 2 to 5 and which continues to the largest  $z = 6.423$  in the sample for which  $z_g = 0.5589$  has been estimated.

high  $z$  ( $z > 2.2$ ) quasar spectra, it would mean that the high redshift quasars necessarily lie along sightlines where the low redshift intervening clouds (detected in the spectra of quasars with  $z < 2$ ) are systematically missing which, if true, would be a cosmic conspiracy. A simpler explanation is that the intervening cloud scenario for the origin of the Mg II absorption lines in the quasar spectrum is not the correct interpretation. In fact, the observed nature of the distribution of  $z_{\text{MgII}}$  (lowest redshift detected in a quasar spectrum) shown in Figure 5a seems to rule out an intervening origin for the Mg II features.

We now investigate the intrinsic origin scenario for the Mg II lines in which the lowest redshift Mg II absorption lines arise within the quasar system and their redshift is the cosmological redshift of the quasar as suggested in the paper. This would necessarily imply that all the spectral lines in a quasar spectrum arise within the quasar and the multiple redshifts contain a contribution from gravitational redshifts as discussed above. Since the gravitational redshift shown by a line photon is a function of the separation of the line forming region from the event horizon of the black hole, the multiple redshifts observed in the quasar spectrum are to be expected as long as photons arise in a region of finite extent located close to the black hole. As the observed  $z$  of the quasar increases, Figure 5a shows that  $z_{\text{MgII}}$  systematically increases with  $z$  and the lowest redshift Mg II features detected in low redshift quasars are never detected in high redshift quasars. In the intrinsic origin,  $z$  will increase either because both  $z_c$  and  $z_g$  have increased or if one of them has increased. Figure 5a shows that  $z_c$  of quasars increases with  $z$  and  $z_c < z$  so that the difference redshift  $z_{\text{in}}$  is due to the effect of an intrinsic physical process i.e. gravitational redshift. Thus, qualitatively, the inclusion of an intrinsic redshift can explain the distribution in Figure 5a. We now quantify  $z_g$  from  $z$  and  $z_c$ . Figure 5b shows the distribution of  $z_g$  with  $z_c = z_{\text{MgII}}$  for the same three catalogues shown in Figure 5a. Interesting results also emerge from this plot. The distribution of the data (Seyffert et al., 2013) in the  $z_c \rightarrow z_g$  plane is rectangular with the upper right corner being sparsely populated. The  $z_g$  estimated for quasars at all  $z_c$  i.e. 0.35 to 2.3 i.e. 0.35 to 2.3 is between 0.0166 and 0.5535 and lines which show  $z_g \geq 0.5$  have to arise from matter inside the ergosphere of the rotating black hole in the quasar. We use these limits to estimate the expected quasar redshifts. The quasar with  $z_c = 0.35$  and  $z_g = 0.5535$  will be detected at  $z = 2.02$  whereas a quasar with  $z_c = 0.35$  and  $z_g = 0.0166$  will be detected at  $z = 0.373$ . The quasar with  $z_c = 2.3$  and  $z_g = 0.5535$  will be detected at  $z = 6.39$  and if  $z_g = 0.0166$ , it will be  $z = 2.355$ . The lower limit of  $z_g = 0.0166$  would be shown by lines forming at a radial separation  $\sim 30$  Schwarzschild radius from the black hole whereas the upper limit of 0.5535 would be shown by lines forming in matter located at 0.903 Schwarzschild radius. In the sample of Seyffert et al. (2013) shown in Figure 5b, the line emitting matter in all the detected quasars is located between these two extremes. The upper limit to  $z_g$  could be indicative of the combination of the rapidly increasing gravitational potential and extreme physics that photons would experience as they emerge from within the ergosphere of the black hole and observational constraints such as observable line widths or redshifts. The paucity of quasars in the top right corner of the rectangular distribution, which is populated by quasars with high  $z_c$  and high  $z_g$  and hence high  $z$  can be explained by the limited number of

quasars detected at high  $z$  (e.g. a quasar with  $z_c = 2.3$  and  $z_g = 0.5535$  which would appear in the top right corner of the distribution will be detected at a redshift  $z = 6.39$ ). Since the sample of quasars in Seyffert et al. (2013) is upto about  $z \sim 5$ , the empty top right hand corner of the rectangular distribution in Figure 5b is easily accounted for by the absence of the high redshift quasars in the catalogue. Considering that the sample of Chen et al. (2016) wherein quasars with  $z > 5.5$  have been targetted does show the presence of a bunch of quasars with  $z_g \sim 0.55$  supports this interpretation and indicates that quasars show the entire range of  $z_g$  at all  $z_c$ . We can, hence, infer that  $z_g$  is independent of  $z_c$  as it should be since  $z_g$  is intrinsic to the quasar and only dependent on black hole physics. A linear decrease in  $z_g$  with increase in  $z_c$  is noticeable in all the three datasets, more so in the higher redshift catalogues. This behaviour is also due to the limited number of high  $z$  quasars in the existing catalogues. The high  $z_c$  quasars (e.g.  $z_c \sim 3$ ) detected within the high  $z$  sample (e.g.  $z \geq 5.5$ ), will necessarily be sensitive to quasars with low  $z_g$  (e.g.  $\sim 0.38$ ). For detecting the high  $z_g$  sample within the high  $z_c$  sample, even higher redshift quasars will have to be targetted. Excepting the lowest  $z_{\text{MgII}}$  in their sample, the catalogues of Matejek & Simcoe (2012); Chen et al. (2016) detect relatively higher redshift Mg II absorption in a catalogue of higher redshift quasars and hence are sensitive to the low  $z_g$  sample. Thus, the distributions in Figure 5a, b are expected if the contribution by gravitational redshift is included. The discussion so far supports the results in the paper and strongly favours the existence of an intrinsic redshift component in addition to a cosmological redshift component in the observed quasar spectra. This model satisfactorily explains observational results from large datasets on quasars without having to resort to any contrived explanations and we believe is the correct interpretation of the quasar spectra.

In Figure 6, the distribution of  $z_g$  with  $z$  of the quasar has been shown. In Figure 6a, the high redshift sample in Matejek & Simcoe (2012); Chen et al. (2016) indicate that the number of quasars in which lines are shifted by a larger  $z_g$  increase with  $z$ . Thus, the high  $z$  of quasars is due to a larger  $z_c$  or  $z_g$  or both as would be expected. The largest  $z_g$  in this sample is 0.563 estimated for a quasar with  $z = 6.31$  and  $z_c = 2.188$ . This  $z_g$  will be shown by lines forming in matter located about 0.888 Schwarzschild radius from the black hole. In Figure 6b, the distribution of  $z_g$  between 0.5 and 0.57 using the quasar data between  $z$  of 0.5 and 6.423 in Raghunathan et al. (2016) has been shown and their appears to be a trend of a gentle increase in the highest detected  $z_g$  with  $z$ . The largest  $z_g$  in this sample is 0.5589 estimated for a quasar with  $z = 6.423$  and  $z_c = 2.274$ . It is not immediately obvious why higher  $z_g$  quasars are not detected at lower  $z_c$ . However we note that data from Seyffert et al. (2013) does not show a trend of increasing  $z_g$  with  $z$  and hence it would be useful to investigate this further before any concrete inferences are drawn.

The above results mean that quasars are not as distant as customarily believed. The highest cosmological redshift detected in the sample of quasar redshifts upto 7.1 (Chen et al., 2016) is 4.778. The proximity of quasars then brings down the enormous luminosities inferred for quasars and will have important implications on several other parameters and models which place quasars at extremely large distances. An interesting point to note is that we can keep detecting quasars at ever increasing emission line redshift for small increases in the gravitational redshift. For example, for quasars at  $z_c = 2$ , the emission line redshifts for  $z_{in} = 1$  (corresponds to  $z_g \sim 0.5$ ) and for  $z_{in} = 2$  (corresponds to  $z_g \sim 0.67$ ) would be  $z = 5$  and  $z = 8$  respectively.  $z_{in}$  and hence  $z$  can keep increasing till  $z_g$  approaches one for the maximally rotating black holes even if there is no increase in  $z_c$  of the quasar. At this juncture, it is instructive to mention that  $z_{in}$  was found well constrained in the paper, which played a major role in convincing the author of a significant contribution by an intrinsic process, because the  $z_g$  of detected quasars was well constrained to values less or around 0.5. We note that  $z_{in}$  can take on a large range of values; for example if  $z_g = 0.5$  then  $z_{in} = 1$ , if  $z_g = 0.9$ , then  $z_{in} = 9$  and if  $z_g = 0.95$  then  $z_{in} = 19$ ! The quasars with  $z_g > 0.5$  that are present in the sample led to  $z_{in}$  being estimated to be  $> 1$  and since the numbers were small, the excess redshift above  $z_{in} = 1$  was incorrectly attributed to the contribution by another unknown intrinsic factor such as Doppler flows. With the correction detailed in point 5, this problem has been removed.

This important edit and examination of more data has only made the case for the intrinsic origin of the entire quasar spectrum and the gravitational redshift origin for the multi-redshifted spectral lines in the quasar spectrum stronger. The observed redshift of the quasar is a combination of cosmological redshift and gravitational redshift of the emission line.

(November 2017)

Table 2: The observed emission line redshift of the quasar, the observed lowest redshift of the Mg II absorption and the estimated gravitational redshifts are noted in columns 2,3,4 respectively for the sample in Matejek & Simcoe (2012) and in columns 6,7,8 for the sample in Chen et al. (2016). The intrinsic redshift ( $z_{\text{in}}$ ) is estimated using the quasar redshift ( $z_{\text{em}}$ ) and the lowest redshift at which Mg II absorption ( $z_{\text{MgII}} = z_c$ ) is detected in the quasar spectrum and the gravitational redshift ( $z_g$ ) is determined using Equation 4. There are upto 8 common quasars in the two catalogues listed here.

Matejek & Simcoe (2012)				Chen et al. (2016)			
Quasar	$z_{\text{em}}$	$z_{\text{MgII}}$	$z_g = z_{\text{in}}/(1 + z_{\text{in}})$	Quasar	$z_{\text{em}}$	$z_{\text{MgII}}$	$z_g = z_{\text{in}}/(1 + z_{\text{in}})$
Q0000-26	4.10	2.184	0.375	SDSSJ0100+2802	6.33	2.326	0.546
BR0004-6224	4.51	2.663	0.335	VIKJ0109-3047	6.79	2.969	0.490
BR0016-3544	4.51	2.783	0.313	PSOJ029-29	5.99	3.609	0.340
SDSS0106+0048	4.45	3.729	0.132	ULASJ0203+0012	5.72	3.711	0.298
SDSS0113-0935	3.67	2.825	0.180	ATLASJ025-33	6.31	2.446	0.528
SDSS0140-0839	3.71	2.241	0.311	VIKJ0305-3150	6.61	2.496	0.540
SDSS0203+0012	5.85	3.711	0.312	PSOJ036+03	6.54	3.275	0.433
BR0305-4957	4.78	2.502	0.394	PSOJ071-02	5.70	2.773	0.436
BR0322-2928	4.62	2.229	0.425	DESJ0454-4448	6.09	2.317	0.532
SDSS0332-0654	3.69	3.061	0.134	PSO065-26	6.14	2.983	0.442
BR0353-3820	4.58	1.987	0.464	PSOJ071-02	5.69	2.773	0.436
BR0418-5723	4.37	2.030	0.435	SDSSJ0818+1722	6.02	3.563	0.35
SDSS0818+1722	5.90	3.563	0.338	SDSSJ0836+0054	5.81	2.299	0.515
SDSS0836+0054	5.82	2.299	0.516	SDSSJ0842+1218	6.07	2.392	0.520
SDSS0949+0335	4.05	2.289	0.348	SDSSJ1030+0524	6.31	2.188	0.563
SDSS1020+0922	3.64	2.046	0.343	J1048-0109	6.64	3.413	0.422
SDSS1030+0524	6.28	2.188	0.562	ULASJ1120+0641	7.09	2.800	0.530
SDSS1110+0244	4.12	2.119	0.390	ULASJ1148+0702	6.32	2.386	0.537
SDSS1305+0521	4.09	2.302	0.351	PSOJ183-12	5.86	2.107	0.547
SDSS1306+0356	5.99	2.533	0.494	SDSSJ1306+0356	6.02	2.533	0.496
ULAS1319+0950	6.13	4.569	0.218	ULAS1319+0950	6.13	4.568	0.219
SDSS1402+0146	4.16	3.277	0.171	SDSSJ1411+1217	5.90	2.237	0.530
SDSS1408+0205	4.01	1.982	0.404	PSOJ213-22	5.92	4.778	0.165
SDSS1411+1217	5.93	2.237	0.532	CFQS1509-1749	6.12	3.127	0.420
Q1422+2309	3.65	3.540	0.023	PSOJ159-02	6.38	2.246	0.560
SDSS1433+0227	4.72	2.772	0.340	PSOJ183+05	6.45	3.207	0.435
CFQS1509-1749	6.12	3.128	0.420	PSOJ209-26	5.72	2.951	0.412
SDSS1538+0855	3.55	2.638	0.200	PSOJ217-16	6.14	2.417	0.521
SDSS1616+0501	4.87	2.741	0.362	VIKJ2211-3206	6.31	3.630	0.366
SDSS1620+0020	4.09	2.910	0.231	PSOJ231-20	6.59	2.419	0.549
SDSS1621-0042	3.7	2.678	0.217	SDSSJ2310+1855	6.00	2.243	0.536
SDSS2147-0838	4.59	2.286	0.412	VIKJ2318-3113	6.51	2.903	0.480
SDSS2228-0757	5.14	3.175	0.320	VIKJ2348-3054	6.90	4.300	0.329
SDSS2310+1855	6.04	2.243	0.539	PSOJ239-07	6.11	4.428	0.236
BR2346-3729	4.21	2.830	0.264	PSOJ242-12	5.83	2.635	0.467